UiO : Department of Mathematics
University of Oslo

The impact of damping and nonlinear modulation on frequency downshift in three dimensional wave trains

May-Iren Espelund

Master's Thesis, Autumn 2022

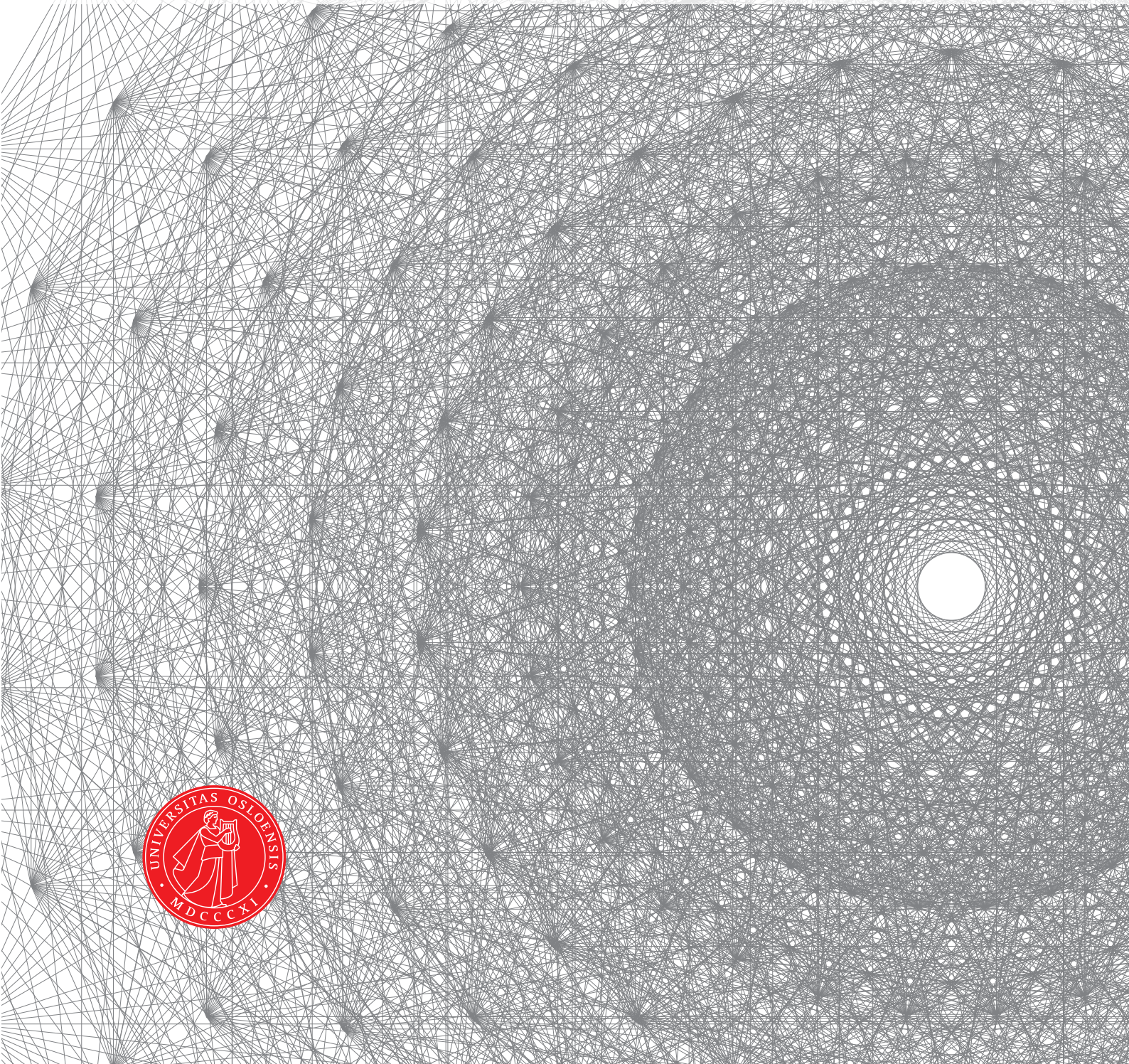

This master's thesis is submitted under the master's programme *Computational Science*, with programme option *Mechanics*, at the Department of Mathematics, University of Oslo. The scope of the thesis is 60 credits.

The front page depicts a section of the root system of the exceptional Lie group E_8, projected into the plane. Lie groups were invented by the Norwegian mathematician Sophus Lie (1842–1899) to express symmetries in differential equations and today they play a central role in various parts of mathematics.

Abstract

We study the evolution of a three dimensional wave train subject to nonlinear modulation and damping. In particular, we are interested in gaining insight about the impact of nonlinear modulation and damping on the frequency downshift that is sometimes observed in three dimensional wave trains. As a motivation for the upcoming simulations, we begin the discussion with the analysis of an experiment that contains both modulation, damping and downshift. Then, starting from the modified nonlinear Schrödinger (MNLS) equation, we add the effects of viscous damping and wave breaking. The equations are solved numerically using a second order multi-component splitting method. The main result is that the non-conservative effects can influence the downshift of the peak; viscous damping may postpone the downshift, while wave breaking may accelerate it.

Acknowledgements

First and foremost, I would like to thank my supervisor Karsten Trulsen for proposing the present thesis for me two years ago. Since then we have had many insightful conversations about the scope of the thesis as well as life in general. You have shared your knowledge with great enthusiasm. I thank my boyfriend Andreas for selflessly taking care of me throughout the years that I have been studying and for making my day-to-day life special. I am grateful for the support of my family and friends and would like to thank my parents in particular for their love and understanding. Finally, I would like to thank my comrades at the study hall for creating an environment that has made the study process enjoyable and fun.

Contents

List of Figures

List of Tables

CHAPTER 1

Introduction

The modulational instability of deep-water uniform wave trains was first discovered by [BF67] back in 1967. They found that these waves are unstable to slow perturbations in space and time, a result that was supported by their own experimental observations. Ten years later, [Lak+77] found experimentally that this modulational instability can lead to a frequency downshift, which can be defined as the downshift of the carrier. Since then, many scientists have tried to explain the various aspects of this phenomenon through experimental observations and simulations. With this latter approach we are able to investigate the evolution of a Stokes wave in the absence of breaking. The two dimensional evolution consists of periodic modulation and demodulation between the carrier and its sidebands [TD97].

Downshift has been documented in two dimensional Stokes waves, only when damping has been introduced into the model. We shall frequently look to [TD90] who implemented the breaking term, that we later employ in this thesis, and found a downshift.

Frequency downshift in three dimensional, short crested wave trains do not require damping. This was shown for the first time by [TD97], using the broader bandwidth modified nonlinear Schrödinger (BMNLS) equation. They anticipated on the basis of the corresponding instability region, that the downshift is dependent on the relative with of the tank. That is, the wavelength of the waves must be sufficiently small compared to the width of the tank before the downshift happens. This observation is important because, more often than not, the tanks that we encounter in the laboratory are not long enough for the phenomena that we want to measure. The only way to increase the effective length of the tank is then to shorten the wavelength of the waves. Sometimes, this is at the expense of the effective width of the tank, which poses a challenge to the ones that wish to study two dimensional, long crested waves.

Laboratory evidence of frequency downshift in a three dimensional wave train was presented for the first time by [TSV99]. In this experiment and in the real world in general, damping is an inevitable part of the evolution of a wave train. This is emphasized in chapter 3 of this thesis. The impact of damping on frequency downshift in three dimensional wave trains is yet to be investigated numerically. In the present thesis, we therefore focus on two main types of damping, namely viscous damping and damping by wave breaking. The models are simple and consist only of a slight adjustment of the conservative MNLS equation.

CHAPTER 2

Theory

2.1 Harmonic analysis

Waves that propagate on the free surface of water are often analyzed in terms of their frequency content. The fundamental assumption that enables this analysis is the idea that the water surface can be constructed from a linear superposition of harmonic wave components of different frequencies, amplitudes, wavelengths and phases. We consider the wave components to be independent of each other, but as waves are nonlinear it should be kept in mind that this is not entirely true. However, for the weakly nonlinear waves that we shall be interested in, this is a rather good approximation. Mathematically, the superposition that we are looking for is achieved by means of a Fourier series or cosine series, which are orthogonal projections of the free surface elevation η onto the function space L^2. To keep it simple, the theory is presented in the following for a general function f.

Orthogonal projection

Let V be a complex Hilbert space with orthogonal basis $\{\psi_0, \ldots, \psi_{N-1}\}$ for some $N \in \mathbb{N}$ and consider a complex function f lying in an ambient Hilbert space W. It is often in our interest to express f as a linear combination of the basis functions of V

$$f \sim \sum_{n=0}^{N-1} \hat{f}_n \psi_n, \tag{2.1}$$

with weights $\hat{f}_n \in \mathbb{C}$. If $f \in V$, this representation is exact and we may replace the symbol "$\sim$" with an equality sign. Moreover it is then well known that the set of weights $\hat{f}_0, \ldots, \hat{f}_{N-1}$ satisfying (2.1) is unique and determined

by the equation

$$\hat{f}_n = \frac{\langle f, \psi_n \rangle}{\|\psi_n\|^2}, \quad n = 0, \ldots, N-1. \tag{2.2}$$

Here and in what follows, $\langle \cdot\,, \cdot \rangle$ and $\|\cdot\|$ denotes the inner product and norm respectively on V, inherited by W. On the contrary, if $f \notin V$ we obviously want to choose the weights so that the error

$$\|f - \sum_{n=0}^{N-1} \hat{f}_n \psi_n\| \tag{2.3}$$

is minimized. It can be shown that this happens whenever the difference in (2.3) is orthogonal to V, that is, whenever

$$\langle f - \sum_{n=0}^{N-1} \hat{f}_n \psi_n, \psi_m \rangle = 0, \quad m = 0, \ldots, N-1, \tag{2.4}$$

which according to the standard rules of the inner product is equivalent to

$$\langle f, \psi_m \rangle = \sum_{n=0}^{N-1} \hat{f}_n \langle \psi_n, \psi_m \rangle, \quad m = 0, \ldots, N-1. \tag{2.5}$$

Due to the orthogonality of the basis $\{\psi_0, \ldots, \psi_{N-1}\}$, the only nonzero term on the right-hand side of (2.5) is the one for which $n = m$. Thus the resulting equations

$$\langle f, \psi_m \rangle = \hat{f}_m \langle \psi_m, \psi_m \rangle = \hat{f}_m \|\psi_m\|^2, \quad m = 0, \ldots, N-1 \tag{2.6}$$

can be solved to yield expressions for the weights $\hat{f}_m$

$$\hat{f}_m = \frac{\langle f, \psi_m \rangle}{\|\psi_m\|^2}, \quad m = 0, \ldots, N-1. \tag{2.7}$$

Comparing this expression to that of (2.2) we see that the precise location of f is irrelevant, at least for the purpose of calculating the weights. With this choise of $\hat{f}_n$, the linear combination (2.1) is what we refer to as the orthogonal projection of f onto V. This will be important in the following.

Fourier series

Let W be the space $L^2([0,T]) = \{f : [0,T] \to \mathbb{C} \mid \int_0^T |f(t)|^2\, dt < \infty\}$ with inner product defined by

$$\langle f, g \rangle_{L^2([0,T])} = \int_0^T f(t) g^*(t)\, dt, \quad f, g \in L^2([0,T]), \tag{2.8}$$

and consider the subspace[1] V spanned by the orthogonal basis functions $\{e^{-\mathrm{i}\omega_n t}\}_{n=-\infty}^{\infty}$ with $\omega_n = n\Delta\omega = \frac{2\pi n}{T}$ and $t \in [0, T]$. The projection of a function $f \in L^2([0,T])$ onto V is then of the form

$$f(t) = \sum_{n=-\infty}^{\infty} \hat{f}_n e^{-\mathrm{i}\omega_n t} = \sum_{n=-\infty}^{\infty} \hat{f}_n e^{-\frac{\mathrm{i}2\pi n t}{T}}. \tag{2.9}$$

In order to find the weights, given by (2.7), we must calculate the inner product of a basis function of V with itself

$$\|e^{-\mathrm{i}\omega_n t}\|^2_{L^2([0,T])} = \langle e^{-\mathrm{i}\omega_n t}, e^{-\mathrm{i}\omega_n t}\rangle_{L^2([0,T])} = \int_0^T e^{-\mathrm{i}\omega_n t} e^{\mathrm{i}\omega_n t}\, dt = \int_0^T dt = T. \tag{2.10}$$

The resulting expression for the weights in (2.9) is then

$$\hat{f}_n = \frac{\langle f, e^{-\mathrm{i}\omega_n t}\rangle_{L^2([0,T])}}{\|e^{-\mathrm{i}\omega_n t}\|^2_{L^2([0,T])}} = \frac{1}{T}\int_0^T f(t) e^{\mathrm{i}\omega_n t}\, dt = \frac{1}{T}\int_0^T f(t) e^{\frac{\mathrm{i}2\pi n t}{T}}\, dt. \tag{2.11}$$

Particularly one property of the Fourier series (2.9) will be important later in the thesis. We can differentiate it two times to obtain

$$f'(t) = \sum_{n=-\infty}^{\infty} (-\mathrm{i}\omega_n)\hat{f}_n e^{-\mathrm{i}\omega_n t} \quad \text{and} \quad f''(t) = \sum_{n=-\infty}^{\infty} (-\mathrm{i}\omega_n)^2 \hat{f}_n e^{-\mathrm{i}\omega_n t} \tag{2.12}$$

from which it follows that

$$\widehat{f'}_n = -\mathrm{i}\omega_n \hat{f}_n \quad \text{and} \quad \widehat{f''}_n = -\omega_n^2 \hat{f}_n. \tag{2.13}$$

These identities come in handy when solving PDEs.

Discrete Fourier transform

In order to implement the representation (2.9) and its corresponding weights (2.11) on a computer, it is necessary that we discretize the time variable t. Let us therefore partition the interval $[0, T]$ into N sub-intervals such that

$$t_j = j\Delta t = \frac{Tj}{N}; \quad j = 0, \ldots, N-1. \tag{2.14}$$

The right endpoint $t_N = T$ is left out under the assumption that $f(0) = f(T)$. With this discretization, we write $f_j = f(t_j)$ and consider both f and the basis functions to be sequences

$$(f_j)_{j=0}^{N-1} \text{ and } (e^{-\mathrm{i}\omega_n t_j})_{j=0}^{N-1}. \tag{2.15}$$

[1] With this particular basis, actually $V = W$.

Let I be a set containing the range of j. The relevant ambient space W is then the sequence space $l^2(I) = \{(f_j)_{j\in I} \in \mathbb{C} \mid \sum_{j\in I} |f_j|^2 < \infty\}$ on which

$$\langle f, g\rangle_{l^2(I)} = \sum_{j=0}^{N-1} f_j g_j^*, \quad f, g \in l^2(I) \tag{2.16}$$

is an inner product. As a result we have

$$\|e^{-\mathrm{i}\omega_n t}\|^2_{l^2(I)} = \langle e^{-\mathrm{i}\omega_n t}, e^{-\mathrm{i}\omega_n t}\rangle_{l^2(I)} = \sum_{j=0}^{N-1} e^{-\mathrm{i}\omega_n t_j} e^{\mathrm{i}\omega_n t_j} = \sum_{j=0}^{N-1} 1 = N, \tag{2.17}$$

and

$$\tilde{f}_n = \frac{\langle f, e^{-\mathrm{i}\omega_n t}\rangle_{l^2(I)}}{\|e^{-\mathrm{i}\omega_n t}\|^2_{l^2(I)}} = \frac{1}{N}\sum_{j=0}^{N-1} f_j e^{\mathrm{i}\omega_n t_j} = \frac{1}{N}\sum_{j=0}^{N-1} f_j e^{\frac{\mathrm{i}2\pi n j}{N}}, \tag{2.18}$$

with $\hat{f}_n$ replaced by $\tilde{f}_n$ in order to emphasize that we are working with a discrete version of (2.7). Equation (2.18) for the computation of the weights is known as the discrete Fourier transform (DFT), which accompanies its inverse (IDFT)

$$f_j = \sum_{n=0}^{N-1} \tilde{f}_n e^{-\mathrm{i}\omega_n t_j} = \sum_{n=0}^{N-1} \tilde{f}_n e^{-\frac{\mathrm{i}2\pi n j}{N}}. \tag{2.19}$$

Cosine series

Let W now be the space $L^2([0, L_y]) = \{f : [0, L_y] \to \mathbb{C} \mid \int_0^{L_y} |f(y)|^2\, dy < \infty\}$ and consider the subspace V spanned by the orthogonal basis functions $\{\cos(k_m y)\}_{m=0}^{\infty}$ with $k_m = m\Delta k = \frac{m\pi}{L_y}$ and $y \in [0, L_y]$. The inner product on V and W is given by (2.8) with t and T replaced by y and L_y respectively. As such, we find that the inner product of a basis function of V with itself is given by

$$\begin{aligned}\|\cos(k_m y)\|^2_{L^2([0,L_y])} &= \langle \cos(k_m y), \cos(k_m y)\rangle_{L^2([0,L_y])} = \int_0^{L_y} \cos^2(k_m y)\, dy \\ &= \frac{1}{2}\int_0^{L_y} (1 + \cos(2k_m y))\, dy = \begin{cases} L_y, & m = 0 \\ \frac{L_y}{2}, & m = 1, 2, 3, \ldots. \end{cases}\end{aligned} \tag{2.20}$$

It follows that the weights, that determine the projection of f onto V

$$f(y) = \sum_{m=0}^{\infty} \hat{f}_m \cos(k_m y) = \sum_{m=0}^{\infty} \hat{f}_m \cos\Big(\frac{m\pi y}{L_y}\Big), \tag{2.21}$$

are given by

$$\hat{f}_m = \frac{\langle f, \cos(k_m y)\rangle_{L^2([0,L_y])}}{\|\cos(k_m y)\|^2_{L^2([0,L_y])}} = \begin{cases} \frac{1}{L_y}\int_0^{L_y} f(y)\,dy, & m = 0 \\ \frac{2}{L_y}\int_0^{L_y} f(y)\cos\left(\frac{m\pi y}{L_y}\right)dy, & m = 1, 2, 3, \ldots. \end{cases} \tag{2.22}$$

Differentiation of the cosine series (2.21) two times yields

$$f''(y) = \sum_{m=0}^{\infty} -k_m^2 \hat{f}_m \cos(k_m y). \tag{2.23}$$

It follows that

$$\widehat{f''}_m = -k_m^2 \hat{f}_m \tag{2.24}$$

which similarly to (2.13) proves useful when solving PDEs.

Discrete Cosine transform

The ideal discretization of the spatial variable y depends strongly on the problem at hand. We shall take into account that we don't necessarily have access to the values of f at the boundaries $y = 0$ and $y = L_y$ and shall accordingly prefer the discretization

$$y_i = (i + 1/2)\Delta y = \frac{(i + 1/2)L_y}{M}; \quad i = 0, \ldots, M-1, \tag{2.25}$$

over a discretization of the form (2.14). With the notation $f_i = f(y_i)$ we again obtain sequences

$$(f_i)_{i=0}^{M-1} \text{ and } (\cos(k_m y_i))_{i=0}^{M-1} \tag{2.26}$$

that lie in the space $l^2(I) = \{(f_i)_{i\in I} \in \mathbb{C} \mid \sum_{i\in I} |f_i|^2 < \infty\}$ where $I = \{0, \ldots, M-1\}$. The proper inner product is given by (2.16) with j and N replaced by i and M respectively. Hence

$$\begin{aligned} \|\cos(k_m y)\|^2_{l^2(I)} = \langle \cos(k_m y), \cos(k_m y)\rangle_{l^2(I)} &= \sum_{i=0}^{M-1} \cos^2(k_m y_i) \\ &= \frac{1}{2}\sum_{i=0}^{M-1}(1 + \cos(2k_m y_i)) = \frac{M}{2} + \frac{1}{4}\sum_{i=0}^{M-1}(e^{\mathrm{i}2k_m y_i} + e^{-\mathrm{i}2k_m y_i}) \\ &= \frac{M}{2} + \frac{1}{4}\sum_{i=0}^{M-1} e^{\frac{\mathrm{i}2\pi m(i+1/2)}{M}} + \frac{1}{4}\sum_{i=0}^{M-1} e^{-\frac{\mathrm{i}2\pi m(i+1/2)}{M}}. \end{aligned} \tag{2.27}$$

The sums in (2.27) are geometric series with common coefficients and ratios $e^{\pm\frac{\mathrm{i}\pi m}{M}}$ and $e^{\pm\frac{\mathrm{i}2\pi m}{M}}$ respectively. Consequently,

$$\|\cos(k_m y)\|^2_{l^2(I)} = \frac{M}{2} + \frac{1}{4}\frac{e^{\frac{\mathrm{i}\pi m}{M}}(1-e^{\mathrm{i}2\pi m})}{1-e^{\frac{\mathrm{i}2\pi m}{M}}} + \frac{1}{4}\frac{e^{-\frac{\mathrm{i}\pi m}{M}}(1-e^{-\mathrm{i}2\pi m})}{1-e^{-\frac{\mathrm{i}2\pi m}{M}}} = \frac{M}{2} \tag{2.28}$$

provided $m \neq 0$. If $m = 0$ we see from (2.27) that

$$\|\cos(k_m y)\|^2_{l^2(I)} = M. \tag{2.29}$$

Whenever we represent the sequence $(f_i)_{i=0}^{M-1}$ by the sum

$$f_i = \sum_{m=0}^{M-1} \tilde{f}_m \cos\Big(\frac{m\pi(i+1/2)}{M}\Big), \tag{2.30}$$

we shall therefore find the coefficients with the formula

$$\tilde{f}_m = \frac{\langle f, \cos(k_m y)\rangle_{l^2(I)}}{\|\cos(k_m y)\|^2_{l^2(I)}} = \begin{cases} \frac{1}{M}\sum_{i=0}^{M-1} f_i, & m = 0 \\ \frac{2}{M}\sum_{i=0}^{M-1} f_i \cos(\frac{m\pi(i+1/2)}{M}), & m = 1,\dots,M-1. \end{cases} \tag{2.31}$$

This equation is known as the discrete cosine transform, which is implemented in MATLAB by the built-in DCT-II function.

2.2 Operator splitting

The evolution equations that we encounter in the simulation of real world events are often complicated and contain terms that describe different physical processes. As often as not, these processes develop at different time and space scales and as such, the processes might require different computational grids and solution methods. Most of the time, we are also faced with nonlinearities that increase the complexity of the evolution equations and the numerical schemes that follow. Once again, different solution methods may be preferable for the linear and nonlinear processes. This motivates the use of an operator splitting method, which is illustrated in the following.

Let x, y and t denote the evolution, space and time variable respectively. The evolution equations that we encounter in this thesis are in general of the form

$$\begin{cases} \frac{\partial f}{\partial x} + (S_1 + \cdots + S_N)f = 0, & \text{for } x \in (0, L_x] \\ f(x,y,t) = f_0(y,t), & \text{at } x = 0, \end{cases} \tag{2.32}$$

where $S_1, \ldots, S_N$ are operators, possibly in space or time, and $f(x, y, t)$ is the solution which is given by the operator exponential

$$f(x, y, t) = e^{-x(S_1 + \cdots + S_N)} f_0(y, t). \tag{2.33}$$

Operator splitting is the idea that an approximation to this solution can be obtained, for any value of x, from a composition of the solutions to the sub-equations

$$\begin{aligned} \frac{\partial f_1}{\partial x} + S_1 f_1 &= 0 \\ &\vdots \\ \frac{\partial f_N}{\partial x} + S_N f_N &= 0. \end{aligned} \tag{2.34}$$

There are many ways to do this. Given a discretization of the of the evolution variable, such as

$$x_k = k\Delta x; \quad \Delta x = \frac{L_x}{K}; \quad k = 0, \ldots, K, \tag{2.35}$$

the most basic approximation scheme is obtained from

$$\begin{cases} f^{k+1} = e^{-\Delta x S_N} \cdots e^{-\Delta x S_1} f^k; & k = 0, \ldots, K-1 \\ f^0 = f_0. \end{cases} \tag{2.36}$$

That is, an approximation f^{k+1} of the exact solution $f(x_{k+1})$ is obtained from solving

$$\begin{cases} \frac{\partial f_n}{\partial x} + S_n f_n = 0, & \text{for } x \in (x_k, x_{k+1}] \\ f_n(x_k) = \delta_{1,n} f^k + (1 - \delta_{1,n}) f_{n-1}(x_{k+1}), \end{cases} \tag{2.37}$$

in order from $n = 1$ to $n = N$ and then setting $f^{k+1} = f_N(x_{k+1})$. If the operators $S_1, \ldots, S_N$ commute, the splitting (2.36) will yield the exact solution. If $S_1, \ldots, S_N$ do not commute, we can determine the accuracy from the operator exponential, defined for a bounded, linear operator[2] S by

$$e^S = \sum_{i=0}^{\infty} \frac{S^i}{i!} = I + S + \frac{1}{2}S^2 + \frac{1}{6}S^3 + \ldots, \tag{2.38}$$

[2]If S is nonlinear, the operator exponential and subsequent treatment of accuracy seems to be more complicated. An interesting take on this can be found in [Sch97]. The results are the same.

where I is the identity operator. Let $N = 2$ for simplicity. The exact solution operator can then be expanded as

$$\begin{aligned} e^{-\Delta x(S_1+S_2)} &= \sum_{i=0}^{\infty} \frac{(-\Delta x(S_1+S_2))^i}{i!} \\ &= I - \Delta x(S_1+S_2) + \frac{(\Delta x)^2}{2}(S_1^2 + S_1S_2 + S_2S_1 + S_2^2) \\ &\quad - \frac{(\Delta x)^3}{6}(S_1^3 + S_1^2S_2 + S_1S_2S_1 + S_1S_2^2 + S_2S_1^2 + S_2S_1S_2 + S_2^2S_1 + S_2^3) \\ &\quad + \mathcal{O}((\Delta x)^4) \end{aligned} \tag{2.39}$$

when S_1 and S_2 are bounded, linear operators. The expansion of the approximate solution operator is, on the other hand,

$$\begin{aligned} e^{-\Delta xS_2}e^{-\Delta xS_1} &= \sum_{i=0}^{\infty} \frac{(-\Delta xS_2)^i}{i!} \sum_{j=0}^{\infty} \frac{(-\Delta xS_1)^j}{j!} = \sum_{p=0}^{\infty}(-\Delta x)^p \sum_{q=0}^{p} \frac{S_2^q S_1^{p-q}}{q!(p-q)!} \\ &= I - \Delta x(S_1+S_2) + \frac{(\Delta x)^2}{2}(S_1^2 + 2S_2S_1 + S_2^2) + \mathcal{O}((\Delta x)^3), \end{aligned} \tag{2.40}$$

where the rightmost sum in the first line is the Cauchy product of the preceding two infinite sums. It is clear that (2.39) and (2.40) do not agree at the second order when S_1 and S_2 don't commute. Therefore, the local error, i.e., the error committed in using the approximation scheme (2.36) at each step Δx, is of second order

$$e^{-\Delta xS_2}e^{-\Delta xS_1}f^k - e^{-\Delta x(S_1+S_2)}f^k = \mathcal{O}((\Delta x)^2). \tag{2.41}$$

The global error, i.e., the error that is accumulated over the entire computational interval $(0, L]$, is thus of order one, which means that (2.36) is a first order scheme.

Better accuracy can be achieved by the symmetric scheme

$$\begin{cases} f^{k+1} = e^{-\frac{\Delta x}{2}S_1}e^{-\frac{\Delta x}{2}S_2}\cdots e^{-\Delta xS_N}\cdots e^{-\frac{\Delta x}{2}S_2}e^{-\frac{\Delta x}{2}S_1}f^k; \quad k = 0, \ldots, K-1 \\ f^0 = f_0, \end{cases} \tag{2.42}$$

which is equivalent to solving

$$\begin{cases} \frac{\partial f_n}{\partial x} + S_n f_n = 0, & \text{for } x \in (x_k, x_{k+1/2}] \\ f_n(x_k) = \delta_{1,n} f^k + (1 - \delta_{1,n}) f_{n-1}(x_{k+1/2}), \end{cases} \tag{2.43}$$

for $n = 1, \ldots, N-1$, then

$$\begin{cases} \frac{\partial f_N}{\partial x} + S_N f_N = 0, & \text{for } x \in (x_k, x_{k+1}] \\ f_N(x_k) = f_{N-1}(x_{k+1/2}), \end{cases} \tag{2.44}$$

and eventually

$$\begin{cases} \frac{\partial f_{N-n}}{\partial x} + S_{N-n} f_{N-n} = 0, & \text{for } x \in (x_{k+1/2}, x_{k+1}] \\ f_{N-n}(x_{k+1/2}) = \delta_{1,n} f_N(x_{k+1}) + (1 - \delta_{1,n}) f_{N-n+1}(x_{k+1}), \end{cases} \tag{2.45}$$

for $n = 1, \ldots, N-1$, and then setting $f^{k+1} = f_1(x_{k+1})$. The expansion of the symmetric solution operator in (2.42) is given by

$$\begin{aligned} e^{-\frac{\Delta x}{2}S_1} e^{-\Delta x S_2} e^{-\frac{\Delta x}{2}S_1} &= \sum_{i=0}^{\infty} \frac{(-\frac{\Delta x}{2}S_1)^i}{i!} \sum_{j=0}^{\infty} \frac{(-\Delta x S_2)^j}{j!} \sum_{l=0}^{\infty} \frac{(-\frac{\Delta x}{2}S_1)^l}{l!} \\ &= \sum_{i=0}^{\infty} \frac{(-\frac{\Delta x}{2}S_1)^i}{i!} \sum_{p=0}^{\infty} (-\Delta x)^p \sum_{q=0}^{p} \frac{S_2^q S_1^{p-q}}{2^{p-q} q!(p-q)!} \\ &= \sum_{r=0}^{\infty} (-\Delta x)^r \sum_{s=0}^{r} \frac{S_1^s}{s!} \sum_{q=0}^{r-s} \frac{S_2^q S_1^{r-s-q}}{2^{r-q} q!(r-s-q)!} \\ &= I - \Delta x(S_1 + S_2) + \frac{(\Delta x)^2}{2}(S_1^2 + S_2 S_1 + S_1 S_2 + S_2^2) \\ &\quad - \frac{(\Delta x)^3}{6}(S_1^3 + \frac{3}{4}S_2 S_1^2 + \frac{3}{2}S_2^2 S_1 + \frac{3}{2}S_1 S_2 S_1 + \frac{3}{2}S_1 S_2^2 + \frac{3}{4}S_1^2 S_2 + S_2^3) \\ &\quad + \mathcal{O}((\Delta x)^4), \end{aligned} \tag{2.46}$$

when $N = 2$ and S_1 and S_2 are bounded, linear operators. A third order local error is then attained whenever S_1 and S_2 don't commute

$$e^{-\frac{\Delta x}{2}S_1} e^{-\Delta x S_2} e^{-\frac{\Delta x}{2}S_1} f^k - e^{-\Delta x(S_1+S_2)} f^k = \mathcal{O}((\Delta x)^3), \tag{2.47}$$

meaning that the symmetric scheme (2.42) is of second order. As this scheme is somewhat more complicated than that of first order, it is natural to use the latter when $S_1, \ldots, S_N$ commute. In the following we refer to (2.36) and (2.42) as the Lie scheme and Strang scheme respectively.

Higher order splitting schemes can be constructed. However, this entails backwards integration with respect to the evolution variable, which often causes the splitting scheme to become unstable [GK96]. For this reason, we will not spend time looking into such methods.

In practice, exact solutions to the sub-equations (2.34) do not always exist. In this case, we must resort to integration schemes that are appropriate for each given equation. Eligible integration schemes can have any order of accuracy, but should at least have the same order as the chosen splitting method when $S_1, \ldots, S_N$ do not commute. This is illustrated in chapter 4 where we make use of the second order explicit Runge-Kutta method

$$f^{k+1} = f^k - \frac{1}{2}\Delta x(Sf^k + S(f^k - \Delta x S f^k)) \tag{2.48}$$

in order to solve one of the sub-equations (2.34) that arise in the Strang splitting of the MNLS equation.

2.3 The model problem

Throughout the thesis we will be concerned with the evolution of gravity waves that propagate on the surface of an incompressible, irrotational and inviscid fluid. On deep water, such waves are described by the BVP

$$\frac{\partial \eta}{\partial t} + \nabla\phi \cdot \nabla\eta = \frac{\partial \phi}{\partial z} \quad \text{at } z = \eta \tag{2.49}$$

$$\frac{\partial \phi}{\partial t} + \frac{1}{2}(\nabla\phi)^2 + g\eta = 0 \quad \text{at } z = \eta \tag{2.50}$$

$$\nabla^2\phi = 0 \quad \text{for } -\infty < z < \eta \tag{2.51}$$

$$\frac{\partial \phi}{\partial z} = 0 \quad \text{at } z = -\infty \tag{2.52}$$

where $\eta = \eta(x, y, t)$ is the surface elevation, $\phi = \phi(x, y, z, t)$ is the velocity potential and g is the gravitational acceleration. The quiescent surface lies in the $xy-$plane, the $z-$axis points vertically upwards and t represents time. This nonlinear BVP can be solved using a perturbation technique under

the presumption that the waves are not too steep. This is equivalent to the requirement that the amplitudes of the waves are not too large compared to the wavelengths. It is therefore natural to quantify steepness in terms of the nondimensional variable $\varepsilon = a_c k_c$, where a_c and k_c is the characteristic amplitude and wavenumber respectively. In order to incorporate this variable into the BVP we normalize all variables by the characteristic amplitude a_c, wavenumber k_c and frequency ω_c according to

$$\begin{aligned} x' =& k_c x \quad y' = k_c y \quad z' = k_c z \quad t' = \omega_c t \\ \eta' = \frac{\eta}{a_c} \quad & \phi' = \frac{k_c}{\omega_c a_c}\phi \quad g' = \frac{k_c}{\omega_c^2} g \end{aligned} \tag{2.53}$$

where the primed variables are normalized and dimensionless. The BVP is then reformulated as

$$\frac{\partial \eta'}{\partial t'} + \varepsilon \nabla' \phi' \cdot \nabla' \eta' = \frac{\partial \phi'}{\partial z'} \quad \text{at } z' = \varepsilon \eta' \tag{2.54}$$

$$\frac{\partial \phi'}{\partial t'} + \frac{1}{2}\varepsilon (\nabla' \phi')^2 + g' \eta' = 0 \quad \text{at } z' = \varepsilon \eta' \tag{2.55}$$

$$\nabla'^2 \phi' = 0 \quad \text{for } -\infty < z' < \varepsilon \eta' \tag{2.56}$$

$$\frac{\partial \phi'}{\partial z'} = 0 \quad \text{at } z' = -\infty, \tag{2.57}$$

from which it is evident that $\varepsilon \ll 1$ serves not only as a measure of steepness but also as a measure of nonlinearity of the waves. In what follows we drop the primes, but keep in mind that the variables are indeed normalized and nondimensional. There is one particular challenge related to the above BVP, namely that the domain itself is dependent on the solution η. It is therefore necessary that we make a Taylor expansion of ϕ about the quiescent surface

$$\phi\Big|_{z=\varepsilon\eta} = \phi\Big|_{z=0} + \varepsilon\eta \frac{\partial \phi}{\partial z}\Big|_{z=0} + \frac{1}{2}\varepsilon^2 \eta^2 \frac{\partial^2 \phi}{\partial z^2}\Big|_{z=0} + \dots, \tag{2.58}$$

which leads to the slightly more complicated BVP

$$\begin{aligned} \frac{\partial \eta}{\partial t} + \varepsilon \nabla \phi \cdot \nabla \eta + \varepsilon^2 \eta \nabla \frac{\partial \phi}{\partial z} \cdot \nabla \eta - \frac{\partial \phi}{\partial z} \\ - \varepsilon \eta \frac{\partial^2 \phi}{\partial z^2} - \frac{1}{2}\varepsilon^2 \eta^2 \frac{\partial^3 \phi}{\partial z^3} = \mathcal{O}(\varepsilon^3) \quad \text{at } z = 0 \end{aligned} \tag{2.59}$$

$$\frac{\partial\phi}{\partial t}+\varepsilon\eta\frac{\partial^2\phi}{\partial t\partial z}+\frac{1}{2}\varepsilon^2\eta^2\frac{\partial^3\phi}{\partial t\partial z^2}+\frac{1}{2}\varepsilon(\nabla\phi)^2 + \varepsilon^2\eta\nabla\phi\cdot\nabla\frac{\partial\phi}{\partial z}+g\eta=\mathcal{O}(\varepsilon^3)\quad\text{at } z=0 \tag{2.60}$$

$$\nabla^2\phi=0\quad\text{for }-\infty<z<0 \tag{2.61}$$

$$\frac{\partial\phi}{\partial z}=0\quad\text{at } z=-\infty. \tag{2.62}$$

We will only be interested in waves whose amplitudes are slowly modulated in space and time compared to the waves themselves. A proper mathematical description of said waves requires the introduction of multiple scales

$$\begin{gathered}x_0=x\quad y_0=y\quad z_0=z\quad t_0=t\\ x_1=\varepsilon x\quad y_1=\varepsilon y\quad z_1=\varepsilon z\quad t_1=\varepsilon t\end{gathered} \tag{2.63}$$

of which x_0, y_0, z_0, t_0 and x_1, y_1, z_1, t_1 are fast- and slow-scales respectively. Let us write

$$\boldsymbol{r}_0=(x_0,y_0,z_0)\quad\boldsymbol{r}_1=(x_1,y_1,z_1)\quad\boldsymbol{x}_0=(x_0,y_0)\quad\boldsymbol{x}_1=(x_1,y_1) \tag{2.64}$$

to simplify the resulting set of equations

$$\frac{\partial\eta}{\partial t_0}+\varepsilon\frac{\partial\eta}{\partial t_1}-\frac{\partial\phi}{\partial z_0}-\varepsilon\frac{\partial\phi}{\partial z_1}+\varepsilon\nabla_{\boldsymbol{x}_0}\phi\cdot\nabla_{\boldsymbol{x}_0}\eta-\varepsilon\eta\frac{\partial^2\phi}{\partial z_0^2}-2\varepsilon^2\eta\frac{\partial^2\phi}{\partial z_0\partial z_1} + \varepsilon^2\nabla_{\boldsymbol{x}_0}\phi\cdot\nabla_{\boldsymbol{x}_1}\eta+\varepsilon^2\nabla_{\boldsymbol{x}_1}\phi\cdot\nabla_{\boldsymbol{x}_0}\eta+\varepsilon^2\eta\nabla_{\boldsymbol{x}_0}\frac{\partial\phi}{\partial z_0}\cdot\nabla_{\boldsymbol{x}_0}\eta - \frac{1}{2}\varepsilon^2\eta^2\frac{\partial^3\phi}{\partial z_0^3}=\mathcal{O}(\varepsilon^3)\quad\text{at } z_0=z_1=0 \tag{2.65}$$

$$\frac{\partial\phi}{\partial t_0}+\varepsilon\frac{\partial\phi}{\partial t_1}+\varepsilon\eta\frac{\partial^2\phi}{\partial z_0\partial t_0}+\varepsilon^2\eta\frac{\partial^2\phi}{\partial t_0\partial z_1}+\varepsilon^2\eta\frac{\partial^2\phi}{\partial t_1\partial z_0}+\frac{1}{2}\varepsilon(\nabla_{\boldsymbol{r}_0}\phi)^2 + \varepsilon^2\nabla_{\boldsymbol{r}_0}\phi\cdot\nabla_{\boldsymbol{r}_1}\phi+\frac{1}{2}\varepsilon^2\eta^2\frac{\partial^3\phi}{\partial t_0\partial z_0^2}+\varepsilon^2\eta\nabla_{\boldsymbol{r}_0}\phi\cdot\nabla_{\boldsymbol{r}_0}\frac{\partial\phi}{\partial z_0} + g\eta=\mathcal{O}(\varepsilon^3)\quad\text{at } z_0=z_1=0 \tag{2.66}$$

$$\nabla^2_{\boldsymbol{r}_0}\phi+2\varepsilon\nabla_{\boldsymbol{r}_0}\cdot\nabla_{\boldsymbol{r}_1}\phi+\varepsilon^2\nabla^2_{\boldsymbol{r}_1}\phi=0\quad\text{for }-\infty<z_0<0,\ -h<z_1<0 \tag{2.67}$$

$$\frac{\partial\phi}{\partial z_0}+\varepsilon\frac{\partial\phi}{\partial z_1}=0\quad\text{at } z_0=-\infty,\ z_1=-h \tag{2.68}$$

whose solution is sought as a perturbation expansion of the form

$$\eta(\boldsymbol{x}_0, \boldsymbol{x}_1, t_0, t_1) = \eta_0(\boldsymbol{x}_0, \boldsymbol{x}_1, t_0, t_1) + \varepsilon\eta_1(\boldsymbol{x}_0, \boldsymbol{x}_1, t_0, t_1) + \varepsilon^2\eta_2(\boldsymbol{x}_0, \boldsymbol{x}_1, t_0, t_1) + \dots$$

$$\phi(\boldsymbol{r}_0, \boldsymbol{r}_1, t_0, t_1) = \phi_0(\boldsymbol{r}_0, \boldsymbol{r}_1, t_0, t_1) + \varepsilon\phi_1(\boldsymbol{r}_0, \boldsymbol{r}_1, t_0, t_1) + \varepsilon^2\phi_2(\boldsymbol{r}_0, \boldsymbol{r}_1, t_0, t_1) + \dots. \tag{2.69}$$

Notice that we let z_1 to be finite despite working with deep water waves. This takes into account that the modulation of the amplitude may be so slow that it effectively happens on shallow water. Upon inserting this expansion into the BVP (2.65-2.68) we obtain one BVP corresponding to every order of the nondimensional variable ε, which allows us to determine $\eta_0, \phi_0, \eta_1, \phi_1, \eta_2, \phi_2, \dots$ recursively. The BVP appearing at the zeroth order $\mathcal{O}(\varepsilon^0)$ is

$$\frac{\partial\eta_0}{\partial t_0} - \frac{\partial\phi_0}{\partial z_0} = 0 \quad \text{at } z_0 = z_1 = 0 \tag{2.70}$$

$$\frac{\partial\phi_0}{\partial t_0} + g\eta_0 = 0 \quad \text{at } z_0 = z_1 = 0 \tag{2.71}$$

$$\nabla^2_{\boldsymbol{r}_0}\phi_0 = 0 \quad \text{for } -\infty < z_0 < 0,\ -h < z_1 < 0 \tag{2.72}$$

$$\frac{\partial\phi_0}{\partial z_0} = 0 \quad \text{at } z_0 = -\infty,\ z_1 = -h \tag{2.73}$$

which is linear in η_0 and ϕ_0. We therefore assume a monochromatic wave of the form

$$\begin{bmatrix}\eta_0\\ \phi_0\end{bmatrix} = \frac{1}{2}\begin{bmatrix}\hat{\eta}_{0,1}\\ \hat{\phi}_{0,1}\end{bmatrix} e^{\mathrm{i}(x_0 - t_0)} + c.c.^3, \tag{2.74}$$

which is a wave travelling in the positive $x-$direction. We determine the slowly modulated amplitudes $\hat{\eta}_{0,1} = \hat{\eta}_{0,1}(\boldsymbol{x}_1, t_1)$ and $\hat{\phi}_{0,1} = \hat{\phi}_{0,1}(z_0, \boldsymbol{r}_1, t_1)$ from the BVP that results from inserting this solution into equations (2.70-2.73)

$$\mathrm{i}\hat{\eta}_{0,1} + \frac{\partial\hat{\phi}_{0,1}}{\partial z_0} = 0 \quad \text{at } z_0 = z_1 = 0 \tag{2.75}$$

$$-\mathrm{i}\hat{\phi}_{0,1} + g\hat{\eta}_{0,1} = 0 \quad \text{at } z_0 = z_1 = 0 \tag{2.76}$$

$$\frac{\partial^2\hat{\phi}_{0,1}}{\partial z_0^2} - \hat{\phi}_{0,1} = 0 \quad \text{for } -\infty < z_0 < 0,\ -h < z_1 < 0 \tag{2.77}$$

$$\frac{\partial\hat{\phi}_{0,1}}{\partial z_0} = 0 \quad \text{at } z_0 = -\infty,\ z_1 = -h. \tag{2.78}$$

[3] c.c. stands for complex conjugate of the previous terms.

From equation (2.77-2.78) it follows that

$$\hat{\phi}_{0,1} = Ae^{z_0} \quad \text{for } -\infty < z_0 < 0,\ -h \le z_1 < 0 \tag{2.79}$$

where $A = A(\boldsymbol{r}_1, t_1)$ is slowly varying in space and time. As a consequence, equations (2.75-2.76) reduce to a linear system for $\hat{\eta}_{0,1}$ and A

$$\begin{bmatrix} \mathrm{i} & 1 \\ g & -\mathrm{i} \end{bmatrix} \begin{bmatrix} \hat{\eta}_{0,1} \\ A \end{bmatrix} = \begin{bmatrix} 0 \\ 0 \end{bmatrix}, \quad \text{at } z_1 = 0 \tag{2.80}$$

which has a nontrivial solution only if the determinant of the coefficient matrix on the left is zero. That is, we require that

$$g = 1, \tag{2.81}$$

which we recognize through (2.53) as the linear dispersion relation for deep water gravity waves

$$\omega_c^2 = gk_c, \quad g \text{ dimensional.} \tag{2.82}$$

As a result, the solution to (2.80) is given by

$$A\Big|_{z_1=0} = -\mathrm{i}\hat{\eta}_{0,1}, \quad \hat{\eta}_{0,1} \text{ free}, \tag{2.83}$$

from which it follows that

$$A = -\mathrm{i}\hat{\eta}_{0,1} f(z_1), \tag{2.84}$$

for some function f that satisfies $f(0) = 1$. Let's write $\hat{\eta}_{0,1} = B$ for simplicity. The fundamental solution to the zeroth order problem is then

$$\begin{bmatrix} \eta_0 \\ \phi_0 \end{bmatrix} = \frac{1}{2} \begin{bmatrix} B \\ -\mathrm{i}Bf(z_1)e^{z_0} \end{bmatrix} e^{\mathrm{i}(x_0 - t_0)} + c.c., \tag{2.85}$$

which implies that the surface elevation η is actually linear to the leading order. We substitute this solution directly into the first order problem $\mathcal{O}(\varepsilon^1)$, which results in

$$\begin{aligned} \frac{\partial \eta_1}{\partial t_0} - \frac{\partial \phi_1}{\partial z_0} &= -\frac{\partial \eta_0}{\partial t_1} + \frac{\partial \phi_0}{\partial z_1} - \nabla_{\boldsymbol{x}_0}\phi_0 \cdot \nabla_{\boldsymbol{x}_0}\eta_0 + \eta_0 \frac{\partial^2 \phi_0}{\partial z_0^2} \\ &= -\frac{1}{2}\Big(\frac{\partial B}{\partial t_1} + \mathrm{i}Bf'(0)\Big)e^{\mathrm{i}(x_0 - t_0)} - \frac{\mathrm{i}}{2}B^2 e^{2\mathrm{i}(x_0 - t_0)} + c.c. \quad \text{at } z_0 = z_1 = 0 \end{aligned} \tag{2.86}$$

$$\begin{aligned}\frac{\partial\phi_1}{\partial t_0}+g\eta_1 &= -\frac{\partial\phi_0}{\partial t_1}-\eta_0\frac{\partial^2\phi_0}{\partial z_0\partial t_0}-\frac{1}{2}(\nabla_{\boldsymbol{r}_0}\phi_0)^2 \\ &= \frac{\mathrm{i}}{2}\frac{\partial B}{\partial t_1}e^{\mathrm{i}(x_0-t_0)}+\frac{1}{4}B^2e^{2\mathrm{i}(x_0-t_0)}+c.c. \quad \text{at } z_0=z_1=0\end{aligned} \tag{2.87}$$

$$\begin{aligned}\nabla^2_{\boldsymbol{r}_0}\phi_1 &= -2\nabla_{\boldsymbol{r}_0}\cdot\nabla_{\boldsymbol{r}_1}\phi_0 \\ &= -\Big(\frac{\partial B}{\partial x_1}f(z_1)-\mathrm{i}Bf'(z_1)\Big)e^{z_0}e^{\mathrm{i}(x_0-t_0)}+c.c. \quad \text{for } -\infty<z_0<0,\ -h<z_1<0\end{aligned} \tag{2.88}$$

$$\frac{\partial\phi_1}{\partial z_0}=-\frac{\partial\phi_0}{\partial z_1}=0 \quad \text{at } z_0=-\infty,\ z_1=-h. \tag{2.89}$$

Since these equations are forced on the right hand side by terms that are proportional to $e^{\pm\mathrm{i}(x_0-t_0)}$ and $e^{\pm2\mathrm{i}(x_0-t_0)}$, it is natural to assume that the solution is of the form

$$\begin{bmatrix}\eta_1\\ \phi_1\end{bmatrix}=\frac{1}{2}\begin{bmatrix}\hat\eta_{1,1}\\ \hat\phi_{1,1}\end{bmatrix}e^{\mathrm{i}(x_0-t_0)}+\frac{1}{2}\begin{bmatrix}\hat\eta_{1,2}\\ \hat\phi_{1,2}\end{bmatrix}e^{2\mathrm{i}(x_0-t_0)}+c.c. \tag{2.90}$$

where the amplitudes depend on the slow scales and $\hat\phi_{1,1}$ and $\hat\phi_{1,2}$ in addition depend on the vertical fast scale. This assumption leads to two additional BVP, one of which is the first harmonic problem

$$\mathrm{i}\hat\eta_{1,1}+\frac{\partial\hat\phi_{1,1}}{\partial z_0}=\frac{\partial B}{\partial t_1}+\mathrm{i}Bf'(0) \quad \text{at } z_0=z_1=0 \tag{2.91}$$

$$-\mathrm{i}\hat\phi_{1,1}+g\hat\eta_{1,1}=\mathrm{i}\frac{\partial B}{\partial t_1} \quad \text{at } z_0=z_1=0 \tag{2.92}$$

$$\frac{\partial^2\hat\phi_{1,1}}{\partial z_0^2}-\hat\phi_{1,1}=-2\Big(\frac{\partial B}{\partial x_1}f(z_1)-\mathrm{i}Bf'(z_1)\Big)e^{z_0} \quad \text{for } -\infty<z_0<0,\ -h<z_1<0 \tag{2.93}$$

$$\frac{\partial\hat\phi_{1,1}}{\partial z_0}=0 \quad \text{at } z_0=-\infty,\ z_1=-h. \tag{2.94}$$

The governing equation and bottom condition for $\hat\phi_{1,1}$ are satisfied by

$$\hat\phi_{1,1}=c_1(\boldsymbol{r_1},t_1)e^{z_0}-\Big(\frac{\partial B}{\partial x_1}f(z_1)-\mathrm{i}Bf'(z_1)\Big)z_0e^{z_0}, \quad \text{for } -\infty<z_0<0,\ -h\le z_1<0, \tag{2.95}$$

from which it follows that the surface conditions constitute an inhomogenous linear system

$$\begin{bmatrix}\mathrm{i} & 1\\ g & -\mathrm{i}\end{bmatrix}\begin{bmatrix}\hat\eta_{1,1}\\ c_1\end{bmatrix}=\begin{bmatrix}\frac{\partial B}{\partial x_1}+\frac{\partial B}{\partial t_1}\\ \mathrm{i}\frac{\partial B}{\partial t_1}\end{bmatrix}, \quad \text{at } z_1=0. \tag{2.96}$$

Due to the dispersion relation (2.81), the coefficient matrix on the left is singular. In order for this system to have a solution we must therefore require that the right-hand side meets a certain criteria. According to the Fredholm alternative, the right-hand side must be orthogonal to the nullspace of the transpose of the coefficient matrix. That is, the system (2.96) has a solution provided

$$\begin{bmatrix} v_1 \\ v_2 \end{bmatrix} \cdot \begin{bmatrix} \frac{\partial B}{\partial x_1} + \frac{\partial B}{\partial t_1} \\ \mathrm{i}\frac{\partial B}{\partial t_1} \end{bmatrix} = 0, \tag{2.97}$$

whenever

$$M^T \boldsymbol{v} = \begin{bmatrix} \mathrm{i} & 1 \\ 1 & -\mathrm{i} \end{bmatrix} \begin{bmatrix} v_1 \\ v_2 \end{bmatrix} = \begin{bmatrix} 0 \\ 0 \end{bmatrix}. \tag{2.98}$$

Since the nullspace of M^T consists of vectors of the form

$$\boldsymbol{v} = c \begin{bmatrix} 1 \\ -\mathrm{i} \end{bmatrix}, \quad c \in \mathbb{C} \tag{2.99}$$

it follows that the solvability condition arising at the first order is the linear advection equation

$$\frac{\partial B}{\partial t_1} + \frac{1}{2}\frac{\partial B}{\partial x_1} = 0. \tag{2.100}$$

In dimensional variables this equation reads

$$\frac{\partial B}{\partial t_1} + \frac{\omega_c}{2k_c}\frac{\partial B}{\partial x_1} = 0, \tag{2.101}$$

which is the statement that within $\mathcal{O}(\varepsilon)$, the leading order amplitude, or envelope, travels with the group velocity $C_g = \frac{\omega_c}{2k_c}$. With this requirement on B we may solve (2.96) for c_1 and continue with the second harmonic problem as well as the higher order problems for $\eta_2, \phi_2, \eta_3, \phi_3, \ldots$. It can be shown that the resulting expression for the surface elevation is

$$\eta(x,y,t) = \frac{1}{2}\Big(B(1-\varepsilon^2\frac{3}{8}B^2)e^{\mathrm{i}(x_0-t_0)} + \varepsilon\frac{1}{2}B^2 e^{2\mathrm{i}(x_0-t_0)} + \varepsilon^2\frac{3}{8}B^3 e^{3\mathrm{i}(x_0-t_0)} + c.c. \Big) \tag{2.102}$$

to third order $\mathcal{O}(\varepsilon^3)$. In the process, several solvability conditions are encountered, including the nonlinear Schrödinger(NLS) equation

$$\frac{\partial B}{\partial t_1} + \frac{1}{2}\frac{\partial B}{\partial x_1} + \varepsilon\Big(\frac{\mathrm{i}}{8}\frac{\partial^2 B}{\partial x_1^2} - \frac{\mathrm{i}}{4}\frac{\partial^2 B}{\partial y_1^2} + \frac{\mathrm{i}}{2}|B|^2 B \Big) = 0, \tag{2.103}$$

and the modified nonlinear Schrödinger(MNLS) equation

$$\frac{\partial B}{\partial t_1} + \frac{1}{2}\frac{\partial B}{\partial x_1} + \varepsilon\Big(\frac{\mathrm{i}}{8}\frac{\partial^2 B}{\partial x_1^2} - \frac{\mathrm{i}}{4}\frac{\partial^2 B}{\partial y_1^2} + \frac{\mathrm{i}}{2}|B|^2 B\Big) \\ - \varepsilon^2\Big(\frac{1}{16}\frac{\partial^3 B}{\partial x_1^3} - \frac{3}{8}\frac{\partial^3 B}{\partial x_1 \partial y_1^2} - \frac{5}{4}|B|^2\frac{\partial B}{\partial x_1} - \frac{1}{4}B\frac{\partial |B|^2}{\partial x_1} - \mathrm{i}B\frac{\partial \bar{\phi}}{\partial x_1}\Big) = 0, \tag{2.104}$$

arising at the second and third order respectively. Both equations are derived under the assumption that the envelope is narrow-banded. To be precise, we require that the bandwidths $\Delta\boldsymbol{k} = (\Delta k_x, \Delta k_y)$ and $\Delta\omega$, which measure the range of wavenumbers and frequencies present in the envelope and thus the modulation scales, is $\mathcal{O}(\varepsilon)$. The MNLS-equation is dependent on the induced slow drift $\bar{\phi} = \bar{\phi}(\boldsymbol{r}_1, t_1)$ appearing in ϕ_3, which satisfies the BVP

$$\frac{\partial \bar{\phi}}{\partial z_1} = \frac{1}{2}\frac{\partial |B|^2}{\partial x_1} \quad \text{at } z_1 = 0 \tag{2.105}$$

$$\frac{\partial^2 \bar{\phi}}{\partial x_1^2} + \frac{\partial^2 \bar{\phi}}{\partial y_1^2} + \frac{\partial^2 \bar{\phi}}{\partial z_1^2} = 0 \quad \text{for } -h < z_1 < 0 \tag{2.106}$$

$$\frac{\partial \bar{\phi}}{\partial z_1} = 0 \quad \text{at } z_1 = -h. \tag{2.107}$$

Solving the MNLS-equation for B therefore includes solving this BVP for $\bar{\phi}$. It is readily observed that, at each order, the solvability condition is a refinement of that at the previous order. The NLS-equation adds linear dispersion and a nonlinear correction of the wavelength to the advection equation (2.100) whilst the MNLS-equation in addition adds nonlinear advection. Both equations are known not only for describing the narrow-banded modulation of weakly nonlinear waves, but also for the insight that they give into the modulational instability of Stokes waves. The Stokes wave train is the permanent, periodic and uniform wave train that is achieved by setting $B = 1$ in (2.102). Before delving into the details of this latter subject however, we will spend some time on adjusting our perspective to that of an experimentalist.

2.4 The experimental approach

When we measure the height of water surface waves in the laboratory, we make use of a measuring device, such as a probe, which remains fixed at

some distance from the wave paddle and tank walls. At its location, the device measures the surface elevation relative to the quiescent surface at discrete instants in time. The result is a time series that we can analyze. If we place multiple measuring devices at increasing distances from the wave paddle, we can investigate how this time series changes as the waves propagate along the tank. The solvability conditions that we encountered in the previous section also provides such insight, but from another perspective. They encourage rather the study of how the waves that we see with the naked eye change in time. For us to be able to compare simulation results to experimental data we must therefore somehow make adjustments to the solvability conditions, so that they agree with the empirical point of view. That is, we need to change the evolution variable of equations (2.103-2.104) from t_1 to x_1. To begin, rewrite the MNLS-equation so that only the desired evolution operator remains on the left hand side

$$\begin{aligned}\frac{\partial B}{\partial x_1} =& -2\frac{\partial B}{\partial t_1} - \frac{\mathrm{i}}{4}\varepsilon\frac{\partial^2 B}{\partial x_1^2} + \frac{\mathrm{i}}{2}\varepsilon\frac{\partial^2 B}{\partial y_1^2} - \mathrm{i}\varepsilon|B|^2 B \\ &+ \frac{1}{8}\varepsilon^2\frac{\partial^3 B}{\partial x_1^3} - \frac{3}{4}\varepsilon^2\frac{\partial^3 B}{\partial x_1 \partial y_1^2} - \frac{5}{2}\varepsilon^2|B|^2\frac{\partial B}{\partial x_1} - \frac{1}{2}\varepsilon^2 B\frac{\partial |B|^2}{\partial x_1} - 2\mathrm{i}\varepsilon^2 B\frac{\partial \bar{\phi}}{\partial x_1}.\end{aligned} \tag{2.108}$$

Our goal is to get rid of all derivatives on the right-hand side, that involve the new evolution operator. Let us therefore replace them by those that are obtained from differentiating equation (2.108). The result is

$$\begin{aligned}\frac{\partial B}{\partial x_1} =& -2\frac{\partial B}{\partial t_1} - \frac{\mathrm{i}}{4}\varepsilon\Big(-2\frac{\partial^2 B}{\partial t_1 \partial x_1} - \frac{\mathrm{i}}{4}\varepsilon\frac{\partial^3 B}{\partial x_1^3} + \frac{\mathrm{i}}{2}\varepsilon\frac{\partial^3 B}{\partial x_1 \partial y_1^2} - 2\mathrm{i}\varepsilon|B|^2\frac{\partial B}{\partial x_1} - \mathrm{i}\varepsilon B^2\frac{\partial B^*}{\partial x_1}\Big) \\ &+ \frac{\mathrm{i}}{2}\varepsilon\frac{\partial^2 B}{\partial y_1^2} - \varepsilon\mathrm{i}|B|^2 B + \frac{1}{8}\varepsilon^2\Big(-2\frac{\partial^3 B}{\partial t_1 \partial x_1^2}\Big) - \frac{3}{4}\varepsilon^2\Big(-2\frac{\partial^3 B}{\partial t_1 \partial y_1^2}\Big) \\ &- \frac{5}{2}\varepsilon^2|B|^2\Big(-2\frac{\partial B}{\partial t_1}\Big) - \frac{1}{2}\varepsilon^2|B|^2\frac{\partial B}{\partial x_1} - \frac{1}{2}\varepsilon^2 B^2\frac{\partial B^*}{\partial x_1} - 2\mathrm{i}\varepsilon^2 B\frac{\partial \bar{\phi}}{\partial x_1} + \mathcal{O}(\varepsilon^3)\end{aligned} \tag{2.109}$$

to which the same procedure is repeated to obtain

$$\begin{aligned}\frac{\partial B}{\partial x_1} =& -2\frac{\partial B}{\partial t_1} - \frac{\mathrm{i}}{4}\varepsilon\Big(-2\Big(-2\frac{\partial B}{\partial t_1^2} - \frac{\mathrm{i}}{4}\varepsilon\frac{\partial^3 B}{\partial t_1\partial x_1^2} + \frac{\mathrm{i}}{2}\varepsilon\frac{\partial^3 B}{\partial t_1\partial y_1^2} - 2\mathrm{i}\varepsilon|B|^2\frac{\partial B}{\partial t_1} - \mathrm{i}\varepsilon B^2\frac{\partial B^*}{\partial t_1}\Big)\\ &- \frac{\mathrm{i}}{4}\varepsilon\Big(-2\frac{\partial^3 B}{\partial t_1\partial x_1^2}\Big) + \frac{\mathrm{i}}{2}\varepsilon\Big(-2\frac{\partial^3 B}{\partial t_1\partial y_1^2}\Big) - 2\mathrm{i}\varepsilon|B|^2\Big(-2\frac{\partial B}{\partial t_1}\Big) - \mathrm{i}\varepsilon B^2\Big(-2\frac{\partial B^*}{\partial t_1}\Big)\Big)\\ &+ \frac{\mathrm{i}}{2}\varepsilon\frac{\partial^2 B}{\partial y_1^2} - \varepsilon\mathrm{i}|B|^2B + \frac{1}{8}\varepsilon^2\Big(-2\frac{\partial^3 B}{\partial t_1\partial x_1^2}\Big) - \frac{3}{4}\varepsilon^2\Big(-2\frac{\partial^3 B}{\partial t_1\partial y_1^2}\Big) - \frac{5}{2}\varepsilon^2|B|^2\Big(-2\frac{\partial B}{\partial t_1}\Big)\\ &- \frac{1}{2}\varepsilon^2|B|^2\Big(-2\frac{\partial B}{\partial t_1}\Big) - \frac{1}{2}\varepsilon^2B^2\Big(-2\frac{\partial B^*}{\partial t_1}\Big) - 2\mathrm{i}\varepsilon^2B\frac{\partial\bar{\phi}}{\partial x_1} + \mathcal{O}(\varepsilon^3).\end{aligned} \tag{2.110}$$

Thankfully, this simplifies to

$$\begin{aligned}\frac{\partial B}{\partial x_1} =& -2\frac{\partial B}{\partial t_1} - \mathrm{i}\varepsilon\frac{\partial^2 B}{\partial t_1^2} + \frac{\mathrm{i}}{2}\varepsilon\frac{\partial^2 B}{\partial y_1^2} - \mathrm{i}\varepsilon|B|^2B\\ &+ \varepsilon^2\frac{\partial^3 B}{\partial t_1\partial y_1^2} + 8\varepsilon^2|B|^2\frac{\partial B}{\partial t_1} + 2\varepsilon^2B^2\frac{\partial B^*}{\partial t_1} - 2\mathrm{i}\varepsilon^2B\frac{\partial\bar{\phi}}{\partial x_1} + \mathcal{O}(\varepsilon^3)\end{aligned} \tag{2.111}$$

which is accurate to the third order. We don't care about higher order terms since that would exceed the accuracy of the MNLS-equation. It then only remains to get rid of the derivative of the induced slow drift. This requires that we make the assumption that also this quantity satisfies the linear advection equation

$$\frac{\partial\bar{\phi}}{\partial t_1} + \frac{1}{2}\frac{\partial\bar{\phi}}{\partial x_1} = 0. \tag{2.112}$$

Moving all terms in (2.111) over to the left-hand side it then follows that

$$\begin{aligned}&\frac{\partial B}{\partial x_1} + 2\frac{\partial B}{\partial t_1} + \varepsilon\Big(\mathrm{i}\frac{\partial^2 B}{\partial t_1^2} - \frac{\mathrm{i}}{2}\frac{\partial^2 B}{\partial y_1^2} + \mathrm{i}|B|^2B\Big)\\ &\quad - \varepsilon^2\Big(\frac{\partial^3 B}{\partial t_1\partial y_1^2} + 8|B|^2\frac{\partial B}{\partial t_1} + 2B^2\frac{\partial B^*}{\partial t_1} + 4\mathrm{i}B\frac{\partial\bar{\phi}}{\partial t_1}\Big) = 0\end{aligned} \tag{2.113}$$

is the desired form of the MNLS-equation. In an analogous manner, we rewrite the surface condition and governing equation for the induced slow

drift as

$$\frac{\partial\bar{\phi}}{\partial z_1} = \frac{1}{2}\frac{\partial|B|^2}{\partial x_1} = \frac{1}{2}\frac{\partial B}{\partial x_1}B^* + \frac{1}{2}B\frac{\partial B^*}{\partial x_1} = -\frac{\partial B}{\partial t_1}B^* - B\frac{\partial B^*}{\partial t_1} = -\frac{\partial|B|^2}{\partial t_1} \quad \text{at } z_1 = 0 \tag{2.114}$$

and

$$4\frac{\partial^2\bar{\phi}}{\partial t_1^2} + \frac{\partial^2\bar{\phi}}{\partial y_1^2} + \frac{\partial^2\bar{\phi}}{\partial z_1^2} = 0 \quad \text{for } -h < z_1 < 0 \tag{2.115}$$

respectively.

Now that the equations agree with the experimental point of view, we can either keep them in their normalized nondimensional form or reintroduce the original dimensional variables. From hereon we will choose the latter alternative, such that the equations that we will analyse and simulate read

$$\frac{\partial B}{\partial x} + \frac{2k_c}{\omega_c}\frac{\partial B}{\partial t} + \frac{\mathrm{i}k_c}{\omega_c^2}\frac{\partial^2 B}{\partial t^2} - \frac{\mathrm{i}}{2k_c}\frac{\partial^2 B}{\partial y^2} + \mathrm{i}k_c^3|B|^2B$$

$$- \frac{1}{\omega_c k_c}\frac{\partial^3 B}{\partial t\partial y^2} - \frac{8k_c^3}{\omega_c}|B|^2\frac{\partial B}{\partial t} - \frac{2k_c^3}{\omega_c}B^2\frac{\partial B^*}{\partial t} - \frac{4\mathrm{i}k_c^3}{\omega_c^2}B\frac{\partial\bar{\phi}}{\partial t} = 0 \quad \text{at } z = 0 \tag{2.116}$$

$$\frac{\partial\bar{\phi}}{\partial z} = -k_c\frac{\partial|B|^2}{\partial t} \quad \text{at } z = 0 \tag{2.117}$$

$$\frac{4k_c^2}{\omega_c^2}\frac{\partial^2\bar{\phi}}{\partial t^2} + \frac{\partial^2\bar{\phi}}{\partial y^2} + \frac{\partial^2\bar{\phi}}{\partial z^2} = 0 \quad \text{for } -h < z < 0 \tag{2.118}$$

$$\frac{\partial\bar{\phi}}{\partial z} = 0 \quad \text{at } z = -h, \tag{2.119}$$

where the first line of the MNLS-equation (2.116) constitutes the NLS-equation.

2.5 Modulational instability of Stokes waves

Perturbations of the uniform wave train appear naturally despite the effort to ensure even the most ideal conditions for our experiments. It is therefore in our interest to see if we can gain any insight through a perturbation analysis of the equations governing the wave train. That is, we want to study how deviations from the Stokes wave, given by

$$B(x,y,t) = B_0 e^{-\mathrm{i}k_c^3|B_0|^2x} \qquad \text{and} \qquad \bar{\phi}(x,y,z,t) = 0, \tag{2.120}$$

behave according to equations (2.116)-(2.119). Let's therefore assume slow perturbations in space and time of the form

$$B(x,y,t) = B_0(1+\alpha(x,y,t)+\mathrm{i}\beta(x,y,t))e^{-\mathrm{i}k_c^3|B_0|^2x}. \tag{2.121}$$

Inserting this into the MNLS equation (2.116), we obtain an equation that can be divided into its real part

$$\begin{aligned}&\frac{\partial\alpha}{\partial x}+\frac{2k_c}{\omega_c}\frac{\partial\alpha}{\partial t}-\frac{k_c}{\omega_c^2}\frac{\partial^2\beta}{\partial t^2}+\frac{1}{2k_c}\frac{\partial^2\beta}{\partial y^2}-k_c^3|B_0|^2(2\alpha+\alpha^2+\beta^2)\beta-\frac{1}{\omega_c k_c}\frac{\partial^3\alpha}{\partial t\partial y^2}\\&\quad-\frac{10k_c^3}{\omega_c}|B_0|^2(1+2\alpha+\alpha^2)\frac{\partial\alpha}{\partial t}-\frac{6k_c^3}{\omega_c}|B_0|^2\beta^2\frac{\partial\alpha}{\partial t}-\frac{4k_c^3}{\omega_c}|B_0|^2(\beta+\alpha\beta)\frac{\partial\beta}{\partial t}\\&\quad+\frac{4k_c^3}{\omega_c^2}\beta\frac{\partial\bar{\phi}}{\partial t}=0\quad\text{at } z=0\end{aligned} \tag{2.122}$$

and its imaginary part

$$\begin{aligned}&\frac{\partial\beta}{\partial x}+\frac{2k_c}{\omega_c}\frac{\partial\beta}{\partial t}+\frac{k_c}{\omega_c^2}\frac{\partial^2\alpha}{\partial t^2}-\frac{1}{2k_c}\frac{\partial^2\alpha}{\partial y^2}+k_c^3|B_0|^2(2\alpha+3\alpha^2+\alpha^3+\beta^2+\alpha\beta^2)\\&\quad-\frac{1}{\omega_c k_c}\frac{\partial^3\beta}{\partial t\partial y^2}-\frac{6k_c^3}{\omega_c}|B_0|^2(1+2\alpha+\alpha^2)\frac{\partial\beta}{\partial t}-\frac{10k_c^3}{\omega_c}|B_0|^2\beta^2\frac{\partial\beta}{\partial t}\\&\quad-\frac{4k_c^3}{\omega_c}|B_0|^2(\beta+\alpha\beta)\frac{\partial\alpha}{\partial t}-\frac{4k_c^3}{\omega_c^2}(1+\alpha)\frac{\partial\bar{\phi}}{\partial t}=0\quad\text{at } z=0.\end{aligned} \tag{2.123}$$

It can be shown that the first five terms of both (2.122) and (2.123) descend from the NLS equation. We also have to take into account, the effect of (2.121) on the induced slow drift $\bar{\phi}$ through equation (2.117), namely

$$\frac{\partial\bar{\phi}}{\partial z}=-2k_c|B_0|^2\Big(\frac{\partial\alpha}{\partial t}+\alpha\frac{\partial\alpha}{\partial t}+\beta\frac{\partial\beta}{\partial t}\Big)\quad\text{at } z=0. \tag{2.124}$$

At this point, it is appropriate to confine ourselves to a linear perturbation analysis by neglecting the nonlinear terms in α, β and $\bar{\phi}$. We then obtain a linear real part

$$\frac{\partial\alpha}{\partial x}+\frac{2k_c}{\omega_c}\frac{\partial\alpha}{\partial t}-\frac{k_c}{\omega_c^2}\frac{\partial^2\beta}{\partial t^2}+\frac{1}{2k_c}\frac{\partial^2\beta}{\partial y^2}-\frac{1}{\omega_c k_c}\frac{\partial^3\alpha}{\partial t\partial y^2}-\frac{10k_c^3}{\omega_c}|B_0|^2\frac{\partial\alpha}{\partial t}=0, \tag{2.125}$$

a linear imaginary part

$$\frac{\partial\beta}{\partial x}+\frac{2k_c}{\omega_c}\frac{\partial\beta}{\partial t}+\frac{k_c}{\omega_c^2}\frac{\partial^2\alpha}{\partial t^2}-\frac{1}{2k_c}\frac{\partial^2\alpha}{\partial y^2}+2k_c^3|B_0|^2\alpha-\frac{1}{\omega_c k_c}\frac{\partial^3\beta}{\partial t\partial y^2}-\frac{6k_c^3}{\omega_c}|B_0|^2\frac{\partial\beta}{\partial t}$$
$$-\frac{4k_c^3}{\omega_c^2}\frac{\partial\bar{\phi}}{\partial t}=0\quad\text{at } z=0, \tag{2.126}$$

as well as a linear surface condition for $\bar{\phi}$

$$\frac{\partial\bar{\phi}}{\partial z}=-2k_c|B_0|^2\frac{\partial\alpha}{\partial t}\quad\text{at } z=0. \tag{2.127}$$

These three equations can be solved by assuming harmonic long wave perturbations of the form

$$\begin{bmatrix}\alpha\\ \beta\\ \bar{\phi}\end{bmatrix}=\begin{bmatrix}\hat{\alpha}\\ \hat{\beta}\\ \hat{\phi}\end{bmatrix}e^{\mathrm{i}(\lambda x+\mu y-\Omega t)}+c.c., \tag{2.128}$$

where $\hat{\phi}$ depends on the vertical scale z. With this assumption, the BVP for $\bar{\phi}$ reduces to a BVP for $\hat{\phi}$

$$\frac{\mathrm{d}\hat{\phi}}{\mathrm{d}z}=2\mathrm{i}k_c|B_0|^2\Omega\hat{\alpha}\quad\text{at } z=0 \tag{2.129}$$

$$\frac{\mathrm{d}^2\hat{\phi}}{\mathrm{d}z^2}-\Big(\frac{4k_c^2\Omega^2}{\omega_c^2}+\mu^2\Big)\hat{\phi}=0\quad\text{for } -h<z<0 \tag{2.130}$$

$$\frac{\mathrm{d}\hat{\phi}}{\mathrm{d}z}=0\quad\text{at } z=-h. \tag{2.131}$$

Equation (2.130) is a linear, second order, homogenous ODE whose general solution is

$$\hat{\phi}(z)=c_1e^{Rz}+c_2e^{-Rz}\quad\text{for } -h<z<0 \tag{2.132}$$

with

$$R=\sqrt{\frac{4k_c^2\Omega^2}{\omega_c^2}+\mu^2}. \tag{2.133}$$

The constants c_1 and c_2 are determined from the boundary conditions (2.129) and (2.131), so that the resulting expression for $\hat{\phi}$ is

$$\hat{\phi}(z) = \frac{2\mathrm{i}k_c|B_0|^2\Omega\cosh(R(z+h))}{R\sinh(Rh)}\hat{\alpha} \quad \text{for } -h \leq z \leq 0. \tag{2.134}$$

Inserting (2.128) into equation (2.125) and (2.126) then leads to the following linear system of equations for $\hat{\alpha}$ and $\hat{\beta}$

$$\begin{bmatrix} \mathrm{i}\lambda - \frac{2\mathrm{i}k_c\Omega}{\omega_c} - \frac{\mathrm{i}\Omega\mu^2}{\omega_c k_c} + \frac{10\mathrm{i}k_c^3|B_0|^2\Omega}{\omega_c} & Q \\ -Q + 2k_c^3|B_0|^2 - \frac{8k_c^4|B_0|^2\Omega^2\coth(Rh)}{\omega_c^2 R} & \mathrm{i}\lambda - \frac{2\mathrm{i}k_c\Omega}{\omega_c} - \frac{\mathrm{i}\Omega\mu^2}{\omega_c k_c} + \frac{6\mathrm{i}k_c^3|B_0|^2\Omega}{\omega_c} \end{bmatrix} \begin{bmatrix} \hat{\alpha} \\ \hat{\beta} \end{bmatrix} = 0 \tag{2.135}$$

where

$$Q = \frac{k_c\Omega^2}{\omega_c^2} - \frac{\mu^2}{2k_c}. \tag{2.136}$$

As the first four and five terms of (2.125) and (2.126) respectively are descendants of the NLS equation, we also find a more manageable system of equations for $\hat{\alpha}$ and $\hat{\beta}$

$$\begin{bmatrix} \mathrm{i}\lambda - \frac{2\mathrm{i}k_c\Omega}{\omega_c} & Q \\ -Q + 2k_c^3|B_0|^2 & \mathrm{i}\lambda - \frac{2\mathrm{i}k_c\Omega}{\omega_c} \end{bmatrix} \begin{bmatrix} \hat{\alpha} \\ \hat{\beta} \end{bmatrix} = 0. \tag{2.137}$$

In order for these systems to have nontrivial solutions, we must require their coefficient matrices to be singular. This is equivalent to the requirement that the determinants of the coefficient matrices are zero, which results in the following growth rates for the perturbation according to the MNLS equation

$$\lambda_{MNLS} = \frac{\left(2k_c^2 + \mu^2 - 8k_c^4|B_0|^2\right)\Omega}{\omega_c k_c} \pm \sqrt{Q\left(Q - 2k_c^3|B_0|^2 + \frac{8k_c^4|B_0|^2\Omega^2\coth(Rh)}{\omega_c^2 R}\right) + \frac{4k_c^6|B_0|^4\Omega^2}{\omega_c^2}} \tag{2.138}$$

and the NLS equation

$$\lambda_{NLS} = \frac{2k_c\Omega}{\omega_c} \pm \sqrt{Q\left(Q - 2k_c^3|B_0|^2\right)}. \tag{2.139}$$

These growth rates are either real or complex valued, depending on the radicands being nonnegative or negative respectively. Looking back at equation (2.128), we see that in the latter case, the perturbations are free to grow exponentially as they propagate along the tank. These are the unstable perturbations of the Stokes wave, whose growth rates are shown in figure (2.1) for $\varepsilon = 0.1$. It is apparent that the imaginary parts of λ_{NLS} and λ_{MNLS}, plotted in figure (2.1a) and (2.1b) respectively, are both symmetric about the origin. As such, neither the lower nor the upper sidebands should dominate the modulation of the Stokes wave in these models. The validity of this interpretation is discussed in section 5, where we analyse the results of a simulation of the two governing equations in question. In figure (2.1a), the level curves of λ_{NLS} are seen to be hyperbolas out of which

$$\Omega^2 - \frac{\omega_c^2}{2k_c^2}\mu^2 = \omega_c^2 k_c^2 |B_0|^2 \tag{2.140}$$

yields the maximum growth rate. The upper part of this hyperbola is represented by dashed lines. There are no such curves on which λ_{MNLS} attains its maximum. We can however locate two isolated points with this property in the limit of infinite depth. In this case the growth rate reaches its maximum for $\mu = 0$ [McL82]. With this in mind, the radicand in (2.138) simplifies to

$$\frac{k_c^2\Omega^4}{\omega_c^4} - \frac{2k_c^4|B_0|^2\Omega^2}{\omega_c^2} + \frac{4k_c^4|B_0|^2|\Omega|^3}{\omega_c^3} + \frac{4k_c^6|B_0|^4\Omega^2}{\omega_c^2}, \tag{2.141}$$

which can be differentiated with respect to Ω to obtain

$$\frac{4k_c^2\Omega^3}{\omega_c^4} - \frac{4k_c^4|B_0|^2\Omega}{\omega_c^2} + \frac{12k_c^4|B_0|^2|\Omega|\Omega}{\omega_c^3} + \frac{8k_c^6|B_0|^4\Omega}{\omega_c^2}. \tag{2.142}$$

The maximum growth rate is achieved by setting this expression to zero, leaving us at the quadratic equation

$$|\Omega|^2 + 3\omega_c k_c^2 |B_0|^2 |\Omega| + 2\omega_c^2 k_c^4 |B_0|^4 - \omega_c^2 k_c^2 |B_0|^2 = 0 \tag{2.143}$$

whose solution is given by

$$|\Omega| = -\frac{3}{2}\omega_c k_c^2 |B_0|^2 + \frac{1}{2}\omega_c k_c |B_0| \sqrt{k_c^2 |B_0|^2 + 4}. \tag{2.144}$$

The two values of Ω satisfying this requirement are both represented by a cross in figure (2.1b). This particular distinction in the growth rates λ_{NLS} and λ_{MNLS} implies that there is a qualitative difference in the modulational

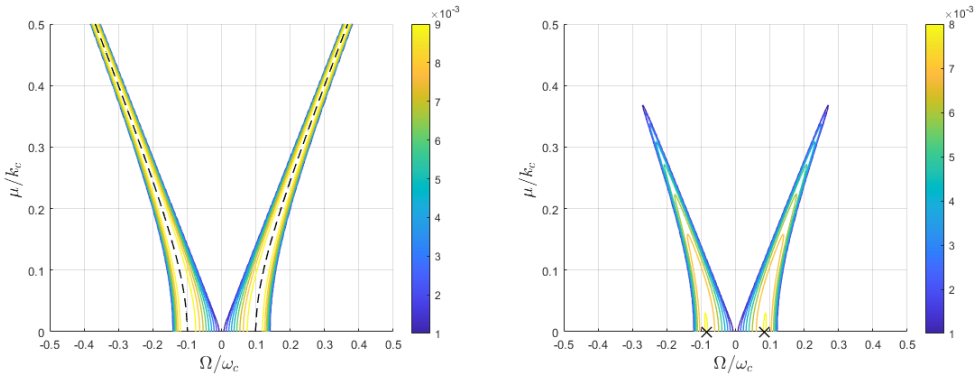

(a) (b)

Figure 2.1: Contour plot indicating the growth rates $\frac{\mathrm{Im}(\lambda)}{k_c}$ for unstable perturbations $(\frac{\Omega}{\omega_c}, \frac{\mu}{k_c})$ in the angular frequency and wavenumber respectively. According to a stability analysis of (a): the NLS equation, the most unstable perturbations: $--$, lie on a hyperbola while according to (b): the MNLS equation, the most unstable perturbations: $\times$, are isolated points. $\varepsilon = 0.1$.

instability governed by the NLS and MNLS equation. While the predominant instabilities are spread out in all three directions according to the NLS equation, its counterpart insists they appear in the direction of propagation. In practice this means that if modulations are free to grow until the point of breaking, then we should see this behaviour largely in the longitudinal direction of the tank. It is also worth noticing from the colorbars of figure (2.1) that the growth rate due to the NLS equation in general is higher than that of the MNLS equation. We keep these remarks in mind when we later on investigate the extent to which the emergence of sidebands in the experimental data from Marintek is in agreement with the instability regions of this section.

CHAPTER 3

Analysis of experimental data

3.1 About the experiment

As a complement to this thesis, access has been given to experimental data collected in 1999 from the towing tank at Marintek, Trondheim, currently known as Sintef Ocean. The data in question are probe measurements of the surface elevation, varying due to the presence of Stokes waves generated at the beginning of a tank of length 260 m and width 10.5 m. Capacitance probes, positioned with the intent of capturing transversal modulations in the wavetrain, were located in groups of five at 10, 80, 120 and 160 meters from the wave paddle. We assume that the amount of waves reflected off the sloping beach at the far end of the tank is negligible[1] so that the measurements are not significantly contaminated. The tank along with the specific arrangement of probes is depicted in figure 3.1. When programming the wave paddle, the height H_0 and period T_0 of the wavetrain were set to 0.1 m and 1.0 s respectively. Through the linear dispersion relation (2.82) we find that this corresponds to the nominal wavenumber

$$k_0 = \frac{4\pi^2}{gT_0^2} = 4.0202 \text{ m}^{-1}, \tag{3.1}$$

where $g = 9.82$ ms^{-2} is the acceleration of gravity. As the depth of the tank was 10 m within the first 80 m of the wave paddle and 5 meters throughout the rest of the tank, the nondimensional depth $k_0 h$ was no less than 20.1. In addition, we roughly estimate the steepness $\epsilon_0 \approx \frac{H_0 k_0}{2} = 0.2010$. These numbers reflect that the waves generated at Marintek were indeed weakly

[1]The nominal period of this experiment is within a range which traditionally is well absorbed by a sloping beach. Besides, as the distance between the probes and the beach was at least about 100 meters, it is probable that viscous damping wore down any reflected waves by the time they arrived at the probes.

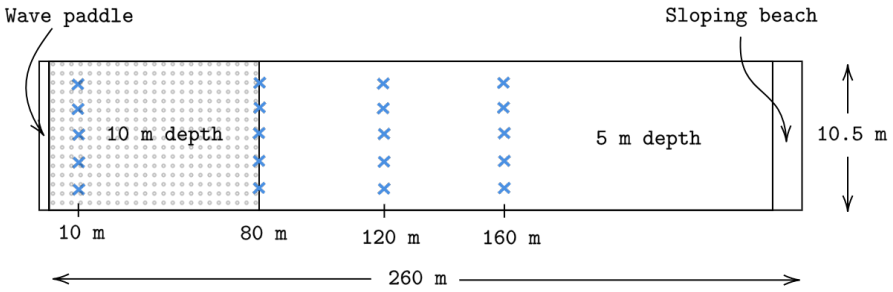

Figure 3.1: The experimental setup: ×, capacitance probes were placed in groups of five at 10, 80, 120 and 160 meters from the wave paddle.

nonlinear, deep water gravity waves, which we know are governed by the equations in section 2.3. We will spend some time analysing the experimental data, in order to get an idea of the kind of behavior that can be expected from a real world Stokes wave.

3.2 Characterizing the experiment

Before embarking on the analysis of the experimental data, we need to know what kind of tools we have at hand. One of the very first things we should know, is whether or not the data exhibits stationarity or homogeneity. In particular we ask if the data are weakly stationary or weakly homogenous as this enables the use of the spectrum. The former property of the data is established through the fact that the wave paddle itself was driven by a weakly stationary signal and through the assumption of negligible reflection off of the beach. In the transversal direction, however, the situation is different. Any modulation in this direction is reflected off the tank walls and weak homogeneity is thus an implausible assumption. Let's calculate the autocorrelation of the data to see if this is a problem or not. The statistical theory that enables the following calculations can be found in the lecture notes written by Professor Karsten Trulsen [Tru22].

In order to estimate the transversal autocorrelation function $R(y_i, y_l)$ at any given distance from the wave paddle, we consider each measurement in time to be a realisation of the stochastic variable $\eta(y_i)$ thereby creating an ensemble $\{\eta_j(y_i)\}_{j=0}^{N-1}$. This allows us to calculate the autocorrelation by

means of an ensemble average

$$R(y_i, y_l) = \mathrm{E}[\eta(y_i)\eta(y_l)] = \frac{1}{N}\sum_{j=0}^{N-1}\eta_j(y_i)\eta_j(y_l) \quad i, l = 0, 1, 2, 3, 4. \tag{3.2}$$

It is however more informative to look at the correlation coefficients $r(y_i, y_l)$ obtained from normalizing the autocorrelation by the standard deviations σ_i and σ_l of the stochastic variables $\eta(y_i)$ and $\eta(y_l)$ respectively. The calculation to be performed for every pair of points y_i, y_l is then

$$r(y_i, y_l) = \frac{\mathrm{E}[\eta(y_i)\eta(y_l)]}{\sigma_i\sigma_l} = \frac{1}{\sigma_i\sigma_l N}\sum_{j=0}^{N-1}\eta_j(y_i)\eta_j(y_l) \quad i, l = 0, 1, 2, 3, 4. \tag{3.3}$$

The results, obtained through a MATLAB implementation, are presented in the tables of figure 3.2. Notice that at any given distance from the wave paddle, the correlation coefficients are symmetric, that is, $r(y_i, y_l) = r(y_l, y_i)$. Moreover, the correlation coefficient of a stochastic variable $\eta(y_i)$ with itself is seen to be roughly equal to unity as expected. In each of the tables, the diagonals represent a deviation in the spatial variable y according to the discretization $\xi_\kappa = \kappa\Delta y$, $\kappa = 0, 1, 2, 3, 4$. For example, both correlation coefficients $r_{10}(y_2, y_4)$ and $r_{10}(y_0, y_2)$ are seen to correspond to a spatial deviation of $\xi_2 = 2\Delta y$. Nevertheless, their numerical values are different. If the data were weakly homogenous, each diagonal would have to contain only identical numbers as this would imply the independence of the autocorrelation function from the absolute position y. Looking at the data, it is clear that this is not the case no matter the distance from the wave paddle. Therefore, we will not be able to compute the spectrum across the tank. We will however employ the spectrum in time in order to estimate the characteristic amplitude a_c.

Unfortunately, we cannot expect that the characteristic variables of the physical wave train are equal to the nominal values that was used to program the wave paddle. In the following, we therefore elaborate on how the characteristic variables are estimated from the experimental data we have at hand. We begin by determining the characteristic angular frequency from the measurements that are closest to the wave paddle. We simply compute the spectrum $\frac{1}{\Delta\omega}|\tilde{\eta}_n(0, y_i)|^2$ of each time series across the tank and locate the peak frequency. From this procedure, we find that the characteristic angular frequency is $\omega_c = 6.2928\ \mathrm{s}^{-1}$. This is slightly larger than the nominal angular frequency $\omega_0 = 2\pi\ \mathrm{s}^{-1}$. The characteristic wavenumber is estimated through the linear dispersion relation

$$k_c = \frac{\omega_c^2}{g} = 4.0325\ \mathrm{m}^{-1} \tag{3.4}$$

r_{10}	y_0	y_1	y_2	y_3	y_4	
y_0	0.9997	0.9932	0.9914	0.9750	0.9890	ξ_4
y_1	0.9932	0.9997	0.9864	0.9697	0.9833	ξ_3
y_2	0.9914	0.9864	0.9997	0.9920	0.9941	ξ_2
y_3	0.9750	0.9697	0.9920	0.9997	0.9888	ξ_1
y_4	0.9890	0.9833	0.9941	0.9888	0.9997	ξ_0

(a)

r_{80}	y_0	y_1	y_2	y_3	y_4	
y_0	0.9997	0.9670	0.8640	0.8227	0.7168	ξ_4
y_1	0.9670	0.9997	0.8627	0.8295	0.7214	ξ_3
y_2	0.8640	0.8627	0.9997	0.9358	0.8212	ξ_2
y_3	0.8227	0.8295	0.9358	0.9997	0.9305	ξ_1
y_4	0.7168	0.7214	0.8212	0.9305	0.9997	ξ_0

(b)

r_{120}	y_0	y_1	y_2	y_3	y_4	
y_0	0.9997	0.8592	0.7058	0.6242	0.5266	ξ_4
y_1	0.8592	0.9997	0.8768	0.7606	0.6705	ξ_3
y_2	0.7058	0.8768	0.9997	0.8648	0.7664	ξ_2
y_3	0.6242	0.7606	0.8648	0.9997	0.9102	ξ_1
y_4	0.5266	0.6705	0.7664	0.9102	0.9997	ξ_0

(c)

r_{160}	y_0	y_1	y_2	y_3	y_4	
y_0	0.9997	0.8281	0.5774	0.5745	0.5996	ξ_4
y_1	0.8281	0.9997	0.7950	0.7165	0.6307	ξ_3
y_2	0.5774	0.7950	0.9997	0.8325	0.6730	ξ_2
y_3	0.5745	0.7165	0.8325	0.9997	0.7802	ξ_1
y_4	0.5996	0.6307	0.6730	0.7802	0.9997	ξ_0

(d)

Figure 3.2: Correlation coefficients $r(y_i, y_l)$ at (a): 10, (b): 80, (c): 120 and (d): 160 meters from the wave paddle. The diagonals represent a deviation in the spatial variable y according to the discretization $\xi_\kappa = \kappa\Delta y,\ \kappa = 0, 1, 2, 3, 4$.

Estimating the characteristic amplitude is a somewhat more involved procedure. We return to the autocorrelation function, this time as a function of the temporal variable t, keeping both spatial variables x and y constant. The definition remains analogous to that of the first equality in (3.2)

$$R(t_j, t_l) = \mathrm{E}[\eta(t_j)\eta(t_l)] \quad j, l = 0, \ldots, N-1. \tag{3.5}$$

Setting the temporal deviation $\tau = t_j - t_l$ to zero we obtain the mean power

$$R(t_j, t_j) = \mathrm{E}[\eta^2(t_j)] = \sum_{n=0}^{N-1} |\tilde{\eta}_n|^2 \tag{3.6}$$

where the second equality is due to the Wiener-Khinchin relations. To leading order, the surface elevation is given by

$$\eta(x_k, y_i, t_j) = a_c \cos(k_c x_k - \omega_c t_j + \theta), \tag{3.7}$$

where the phase θ is assumed to be uniformly distributed[2] over the interval

[2]It is pointed out in [Hol07] that "For most wave records, the phases turn out to have any value between 0 and 2π without any preference for any one value...this is almost always the case in deep water"(p. 31).

$[0, 2\pi]$. We can then calculate the expected value

$$\begin{aligned}\mathrm{E}[\eta^2(t_j)] &= \mathrm{E}[a_c^2 \cos^2(k_c x_k - \omega_c t_j + \Theta)] = \frac{a_c^2}{2\pi}\int_0^{2\pi} \cos^2(k_c x_k - \omega_c t_j + \theta)\, d\theta \\ &= \frac{a_c^2}{4\pi}\int_0^{2\pi} \Big(1 + \cos(2k_c x_k - 2\omega_c t_j + 2\theta)\Big)\, d\theta \\ &= \frac{a_c^2}{2} + \frac{a_c^2}{8\pi}\sin(2k_c x_k - 2\omega_c t_j + 2\theta)|_0^{2\pi} = \frac{a_c^2}{2}\end{aligned} \tag{3.8}$$

From (3.6) and (3.8) it then follows that the characteristic amplitude can be estimated by

$$a_c = \sqrt{2\sum_{n=0}^{N-1} |\tilde{\eta}_n|^2} \tag{3.9}$$

at each of the first five probes. Upon taking the average of the five resulting values we find that

$$a_c = 0.0522 \text{ m} \tag{3.10}$$

and

$$\epsilon = a_c k_c = 0.2105. \tag{3.11}$$

It is seen that all the estimated characteristic variables are greater than the corresponding nominal variables. This is a common observation for a wave that is generated in the laboratory. We also find that the relative width of the tank is

$$\Delta\mu_0 = 0.0744. \tag{3.12}$$

Thus, we should expect to see some modulation to transversal sidebands.

3.3 Energy estimates and distributions

It is through analysing the energy content of the waves that we are able to gain insight about their evolution as they propagate along the tank. In practice, such an analysis is a deep dive into the frequency content of the waves. In this section we will therefore analyse the distribution of energy across longitudinal and transversal modes[3] and examine how this distribution changes with an ever increasing distance from the wave paddle.

[3]When speaking about transversal modes we are really referring to the transversal wavenumber k.

It is natural to begin with the discretization of the surface elevation $\eta(x, y, t)$. At a given distance x from the wavemaker, we consider the continuous, harmonic representation of $\eta(y, t)$ as

$$\eta(y,t) = \sum_{n=-\infty}^{\infty} \sum_{m=0}^{\infty} \tilde{\eta}_{m,n} \cos(k_m y) e^{-\mathrm{i}\omega_n t}, \tag{3.13}$$

with

$$k_m = \frac{m\pi}{L_y} \quad \text{and} \quad \omega_n = \frac{2\pi n}{T}. \tag{3.14}$$

The dependency of η and $\tilde{\eta}_{m,n}$ on longitudinal position x is left out for simplicity. Let us also, for the time being, fix the transversal position y and focus our attention on the behaviour of the surface elevation in time. We then allow ourselves to write

$$\eta(y,t) = \sum_{n=-\infty}^{\infty} \tilde{\zeta}_n(y) e^{-\mathrm{i}\omega_n t}, \tag{3.15}$$

with

$$\tilde{\zeta}_n(y) = \sum_{m=0}^{\infty} \tilde{\eta}_{m,n} \cos(k_m y). \tag{3.16}$$

We place the computational grid t_j in time so that it coincides with the sampling rate of the probes (20 Hz)

$$t_j = j\Delta t = \frac{jT}{N}; \quad j = 0, \ldots, N-1; \quad N = 3914. \tag{3.17}$$

As this grid is finite, the summation in (3.15) must naturally be finite as well and the semi-discrete surface elevation become

$$\eta_j(y) = \sum_{n=0}^{N-1} \tilde{\zeta}_n(y) e^{-\frac{\mathrm{i}2\pi n j}{N}}. \tag{3.18}$$

The resulting discrete basis functions $e^{-\frac{\mathrm{i}2\pi n j}{N}}$ are orthogonal according to our calculations in section 2.1, from which we recall that

$$\left\langle e^{-\frac{\mathrm{i}2\pi n j}{N}}, e^{-\frac{\mathrm{i}2\pi q j}{N}} \right\rangle_{l^2} = \sum_{j=0}^{N-1} e^{-\frac{\mathrm{i}2\pi (n-q) j}{N}} = \begin{cases} 0, & n \neq q \\ N, & n = q. \end{cases} \tag{3.19}$$

We can now estimate the energy per unit time or mean power for fixed x and y as follows

$$\begin{aligned}\frac{1}{N}\sum_{j=0}^{N-1}\eta_j^2 = \frac{1}{N}\sum_{j=0}^{N-1}\eta_j\eta_j^* &= \frac{1}{N}\sum_{j=0}^{N-1}\left(\sum_{n=0}^{N-1}\tilde{\zeta}_n e^{-\frac{\mathrm{i}2\pi nj}{N}}\right)\left(\sum_{q=0}^{N-1}\tilde{\zeta}_q e^{-\frac{\mathrm{i}2\pi qj}{N}}\right)^* \\ &= \frac{1}{N}\sum_{j=0}^{N-1}\left(\sum_{n=0}^{N-1}\tilde{\zeta}_n e^{-\frac{\mathrm{i}2\pi nj}{N}}\right)\left(\sum_{q=0}^{N-1}\tilde{\zeta}_q^* e^{\frac{\mathrm{i}2\pi qj}{N}}\right) \\ &= \frac{1}{N}\sum_{j=0}^{N-1}\sum_{n,q=0}^{N-1}\tilde{\zeta}_n\tilde{\zeta}_q^* e^{-\frac{\mathrm{i}2\pi(n-q)j}{N}} = \frac{1}{N}\sum_{n,q=0}^{N-1}\tilde{\zeta}_n\tilde{\zeta}_q^*\sum_{j=0}^{N-1}e^{-\frac{\mathrm{i}2\pi(n-q)j}{N}} \\ &\overset{(3.19)}{=} \sum_{n=0}^{N-1}\tilde{\zeta}_n\tilde{\zeta}_n^*.\end{aligned} \tag{3.20}$$

This result is an instance of the famous theorem of Parseval. If the waves were long crested, this latter expression would give an estimate for the average energy per unit horizontal surface area. Taking the transversal modulation of the waves into account, we however discover that this expression is insufficient to describe energy distribution across modes. Therefore, we need to take an average of the acquired expression in (3.20) over an appropriate transversal grid.

If we try to discretize y according to the positioning of the probes, we quickly run into problems. It turns out that this grid

$$y_i = \frac{(i+1)L_y}{M}; \quad i = 0, \dots, M-2; \quad M = 6 \tag{3.21}$$

is incompatible with orthogonality of the basis functions $\cos(k_m y_i)$. Specifically, it can be shown that

$$\begin{aligned}\Big\langle \cos\Big(\frac{m\pi(i+1)}{M}\Big), \cos\Big(\frac{p\pi(i+1)}{M}\Big)\Big\rangle_{l^2} &= \sum_{i=0}^{M-2}\cos\Big(\frac{m\pi(i+1)}{M}\Big)\cos\Big(\frac{p\pi(i+1)}{M}\Big) \\ &= \begin{cases} 0, & m \neq p,\ m-p \text{ is odd} \\ -4, & m \neq p,\ m-p \text{ is even} \\ \frac{1}{2}(M-2), & m = p \neq 0 \\ 4(M-1), & m = p = 0. \end{cases}\end{aligned} \tag{3.22}$$

If we were to ignore the lack of orthogonality[4] and carry on with the calculation of energy, the resulting description would contain terms with products of different modes. Such a description does not contribute to physical insight into the experiment, as it invalidates the visual inferences that we would like to make based on the harmonic components of η. Therefore, to tackle this problem, we need another configuration of the transversal grid y_i. The most convenient one is

$$y_i = \frac{(i+1/2)L_y}{M}; \quad i = 0, \dots, M-1; \quad M = 6 \tag{3.23}$$

whose corresponding basis functions are orthogonal with respect to the l^2 inner product

$$\sum_{i=0}^{M-1} \cos\Big(\frac{m\pi(i+1/2)}{M}\Big) \cos\Big(\frac{p\pi(i+1/2)}{M}\Big) = \begin{cases} 0, & m \neq p \\ \frac{M}{2}, & m = p \neq 0 \\ M, & m = p = 0 \end{cases} \tag{3.24}$$

as we have already seen in section 2.1. This grid has the same spatial step $\Delta y = \frac{L_y}{M}$, but is shifted a distance $\frac{\Delta y}{2}$ to the left and consists of an extra point. To retrieve this extra point we still have to make use of the nonorthogonal basis above. Therefore, let us first make a discretization of (3.16) in terms of (3.21)

$$\tilde{\zeta}_n(y_i) = \sum_{m=0}^{M-2} \tilde{\eta}_{m,n} \cos\Big(\frac{m\pi(i+1)}{M}\Big); \quad i = 0, \dots, M-2; \quad M = 6 \tag{3.25}$$

for fixed n. This is a linear system of equations

$$\begin{bmatrix} \tilde{\zeta}_n(y_0) \\ \tilde{\zeta}_n(y_1) \\ \tilde{\zeta}_n(y_2) \\ \tilde{\zeta}_n(y_3) \\ \tilde{\zeta}_n(y_4) \end{bmatrix} = \begin{bmatrix} 1 & \frac{\sqrt{3}}{2} & \frac{1}{2} & 0 & -\frac{1}{2} \\ 1 & \frac{1}{2} & -\frac{1}{2} & -1 & -\frac{1}{2} \\ 1 & 0 & -1 & 0 & 1 \\ 1 & -\frac{1}{2} & -\frac{1}{2} & 1 & -\frac{1}{2} \\ 1 & -\frac{\sqrt{3}}{2} & \frac{1}{2} & 0 & -\frac{1}{2} \end{bmatrix} \begin{bmatrix} \tilde{\eta}_{0,n} \\ \tilde{\eta}_{1,n} \\ \tilde{\eta}_{2,n} \\ \tilde{\eta}_{3,n} \\ \tilde{\eta}_{4,n} \end{bmatrix} \tag{3.26}$$

[4]Effort has been made to find a weighted inner product with respect to which the functions $\cos\big(\frac{m\pi(i+1)}{M}\big)$ are orthogonal, but the attempt resulted in a trivial solution for the weights. The problem is presumably that one missing point.

from which we calculate the coefficients $\tilde{\eta}_{m,n}$ by inverting the matrix

$$\begin{bmatrix} \tilde{\eta}_{0,n} \\ \tilde{\eta}_{1,n} \\ \tilde{\eta}_{2,n} \\ \tilde{\eta}_{3,n} \\ \tilde{\eta}_{4,n} \end{bmatrix} = \begin{bmatrix} \frac{1}{3} & 0 & \frac{1}{3} & 0 & \frac{1}{3} \\ \frac{\sqrt{3}}{3} & 0 & 0 & 0 & -\frac{\sqrt{3}}{3} \\ \frac{1}{2} & -\frac{1}{2} & 0 & -\frac{1}{2} & \frac{1}{2} \\ \frac{\sqrt{3}}{6} & -\frac{1}{2} & 0 & \frac{1}{2} & -\frac{\sqrt{3}}{6} \\ \frac{1}{6} & -\frac{1}{2} & \frac{2}{3} & -\frac{1}{2} & \frac{1}{6} \end{bmatrix} \begin{bmatrix} \tilde{\zeta}_n(y_0) \\ \tilde{\zeta}_n(y_1) \\ \tilde{\zeta}_n(y_2) \\ \tilde{\zeta}_n(y_3) \\ \tilde{\zeta}_n(y_4) \end{bmatrix}. \tag{3.27}$$

Returning to the continuous description (3.16) of $\tilde{\zeta}_n$, we see that we obtain an interpolation from which we are able to make the approximation

$$\tilde{\zeta}_n(y) \approx \sum_{m=0}^{M-2} \tilde{\eta}_{m,n} \cos(k_m y); \quad M = 6 \tag{3.28}$$

provided there is no aliasing. This expression is exact when y coincides with (3.21), while the desired orthogonality properties are achieved by inserting (3.23)

$$\tilde{\zeta}_n(y_i) \approx \sum_{m=0}^{M-2} \tilde{\eta}_{m,n} \cos\Big(\frac{m\pi(i+1/2)}{M}\Big); \quad i = 0, \ldots, M-1; \quad M = 6. \tag{3.29}$$

Finally then, we are ready to take the summation of (3.20) over the

transversal grid

$$\begin{aligned}
\bar{E} &:= \frac{1}{N}\frac{1}{M}\sum_{i=0}^{M-1}\sum_{j=0}^{N-1}\eta_{i,j}^2 \overset{(3.20)}{=} \frac{1}{M}\sum_{i=0}^{M-1}\sum_{n=0}^{N-1}\tilde{\zeta}_n(y_i)\tilde{\zeta}_n(y_i)^* \\
&\overset{(3.29)}{\approx} \frac{1}{M}\sum_{i=0}^{M-1}\sum_{n=0}^{N-1}\left(\sum_{m=0}^{M-2}\tilde{\eta}_{m,n}\cos\Big(\frac{m\pi(i+1/2)}{M}\Big)\right)\left(\sum_{p=0}^{M-2}\tilde{\eta}_{p,n}\cos\Big(\frac{p\pi(i+1/2)}{M}\Big)\right)^* \\
&= \frac{1}{M}\sum_{i=0}^{M-1}\sum_{n=0}^{N-1}\left(\sum_{m=0}^{M-2}\tilde{\eta}_{m,n}\cos\Big(\frac{m\pi(i+1/2)}{M}\Big)\right)\left(\sum_{p=0}^{M-2}\tilde{\eta}_{p,n}^*\cos\Big(\frac{p\pi(i+1/2)}{M}\Big)\right) \\
&= \frac{1}{M}\sum_{i=0}^{M-1}\sum_{n=0}^{N-1}\sum_{m,p=0}^{M-2}\tilde{\eta}_{m,n}\tilde{\eta}_{p,n}^*\cos\Big(\frac{m\pi(i+1/2)}{M}\Big)\cos\Big(\frac{p\pi(i+1/2)}{M}\Big) \\
&= \frac{1}{M}\sum_{n=0}^{N-1}\sum_{m,p=0}^{M-2}\tilde{\eta}_{m,n}\tilde{\eta}_{p,n}^*\sum_{i=0}^{M-1}\cos\Big(\frac{m\pi(i+1/2)}{M}\Big)\cos\Big(\frac{p\pi(i+1/2)}{M}\Big) \\
&\overset{(3.24)}{=} \frac{1}{2}\sum_{n=0}^{N-1}\sum_{m,p=0}^{M-2}\tilde{\eta}_{m,n}\tilde{\eta}_{p,n}^*\delta_{m,p}(1+\delta_{0,p}) = \frac{1}{2}\sum_{n=0}^{N-1}\sum_{m=0}^{M-2}\tilde{\eta}_{m,n}\tilde{\eta}_{m,n}^*(1+\delta_{0,m}) \\
&= \frac{1}{2}\sum_{n=0}^{N-1}\sum_{m=0}^{M-2}|\tilde{\eta}_{m,n}|^2(1+\delta_{0,m}) = \sum_{n=0}^{N-1}\sum_{m=0}^{M-2}\bar{E}_{m,n}.
\end{aligned} \tag{3.30}$$

We see that the estimate for the average energy[5] per unit horizontal surface area reduces to a weighted sum of the square of the coefficients in the harmonic expansion of η. This expression is used extensively in the following, both in the analysis of experimental results and in the subsequent simulations.

3.4 The evolution of a physical Stokes wave

Throughout the rest of the thesis, we will frequently be interested in how energy is distributed across modes. There are many ways to visualize this. A natural option is to plot $\bar{E}_{m,n}$ against ω_n and k_m on a three dimensional axis,

[5]Strictly speaking, to obtain the actual energy we would have to multiply (3.30) by ρg. We choose to overlook this detail as it is immaterial for the distribution of energy across modes.

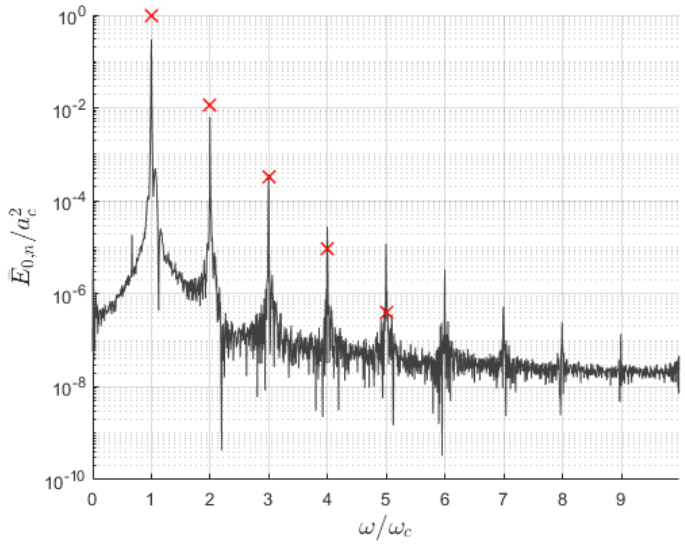

Figure 3.3: Energy distribution across longitudinal modes for $k_m = 0$ at 10 meters from the wave paddle. The first five contributions to the corresponding distribution of an unperturbed Stokes wave: ×, is included.

like we have done with the experimental data in figure (3.4) for the relevant values of x. However, to accentuate that we are dealing with the evolution of a Stokes wave, we can plot the energy distribution at the first set of probes for $k_m = 0$ on a semi-logarithmic axis, like the one in figure (3.3). The corresponding plots for $k_m \neq 0$ are insignificant, as their contribution to the energy at this stage is negligible. The energy in the first five harmonics of an unperturbed Stokes wave, as obtained from [Fen85], is also illustrated in the figure with the red crosses. They are seen to deviate somewhat from the experimental results. This is an indication that perturbations have grown significantly by the time the waves reach the first set of probes, and started the modulation process. The data exhibits nonetheless the same pattern as that of an unperturbed Stokes wave; the spikes of energy occur at integer multiples of the characteristic frequency and their intensity decreases as we move along the horizontal axis.

Let's look into how this Stokes wave evolves during its course along the tank. For this purpose, we return to figure (3.4) in which the energy distribution $\bar{E}_{m,n}$ is plotted over the instability region of the NLS equation at various distances from the wave paddle. At the beginning of its course, the wavetrain is seen to carry essentially all energy in the characteristic frequency. Transversal modes are yet to appear, at least macroscopically. It is well known that this uniform configuration is unstable. Indeed there is no

doubt, judging from figure (3.4b), that by the time the waves arrive at the second set of probes, they have undergone modulation to the extent that we can no longer state that they are regular. Although the peak remains unchanged, we see that a vast amount of its energy is redistributed to both lower and upper frequency sidebands as well as transversal modes. From this moment on, the contribution from nonzero wavenumbers to the total energy is thus important, which furthermore suggests that the waves have become short crested. Figure (3.4c) shows that a lot happens during the next 40 meters. The peak in the energy distribution is seen not only to be downshifted from the characteristic frequency, but also to be much smaller than it was before. This trend continues as the now highly irregular wavetrain passes the final set of probes. The previous remarks are supported

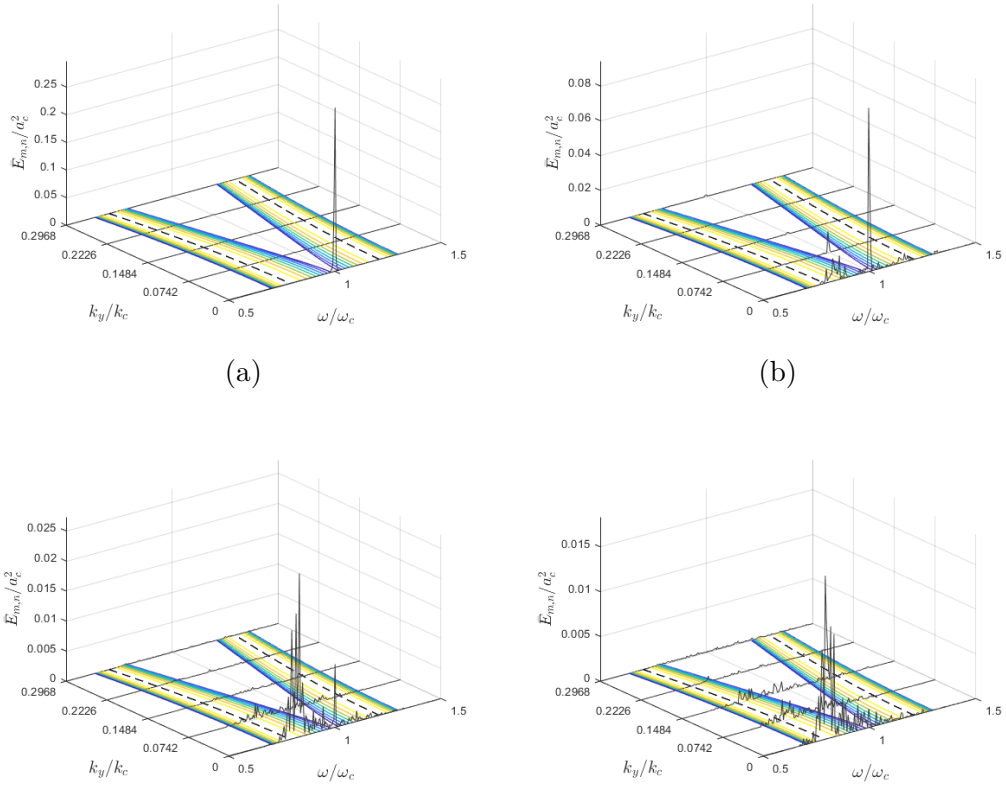

(a) (b)

(c) (d)

Figure 3.4: Energy distribution across longitudinal and transversal modes at (a): 10, (b): 80, (c): 120 and (d): 160 meters from the wave paddle. The instability region of the NLS equation, calculated in section 2.5, is included for comparison.

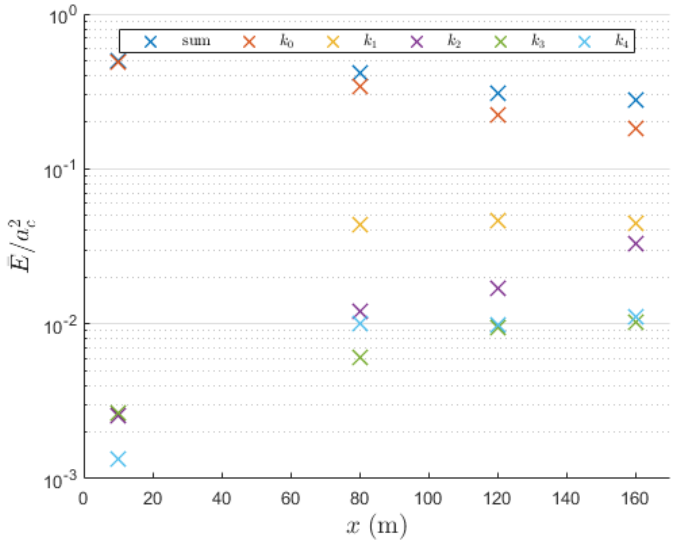

Figure 3.5: Distribution of energy across transversal modes with increasing distance from the wave paddle. The total energy is included as a reference.

by figure (3.5), in which the transversal energy distribution

$$\bar{E}_m = \sum_{n=0}^{N-1} \bar{E}_{m,n}; \quad m = 0, \ldots, M-2 \tag{3.31}$$

is plotted on a semi-logarithmic axis. It is worth noticing from this figure that the energy distribution is not entirely monotonic with respect to the wavenumber k.

The preceding observations do not exactly fit the narrative of the instability region of the NLS equation. The symmetric growth of sidebands, that is anticipated about the characteristic frequency in the second order theory, is not present in the experimental data. In fact, the upper sidebands are barely noticeable compared to the lower ones. In addition, the emergence of oblique sidebands is not at all uniform. Instead, it seems like the short transverse wave components receive less energy than the long ones. The energy distribution across the lower, two dimensional sidebands show nonetheless decent conformity with the theoretical growth rates. Similar remarks can be made from figure (3.6), in which the energy distribution is plotted over the instability region of the MNLS equation. From this figure alone, we might conclude that also the third order theory fails to foresee the asymmetric growth of sidebands. We will see later on that this actually is not the case. There is no doubt, however, that the nonuniform growth of oblique sidebands is much better represented with this increasingly accurate

theory. It should be kept in mind that although the energy distribution is presented together with these instability regions, a direct comparison between them is not really valid beyond the second set of probes; this is due to the findings of section (2.5) only being valid in the early stages of modulation. The instability regions are therefore only expected to say something about the general behaviour of the modulated waves. Yet, figure (3.6b) demonstrates that the most unstable lower sideband is effectively reproduced by the MNLS equation as far as 80 meters from the wave paddle.

Figure (3.5) indicates that the evolution of the wavetrain is nonconservative in nature. Indeed, the waves seem to have lost over one third of their energy by the time they reach the far end of the tank. The reason for

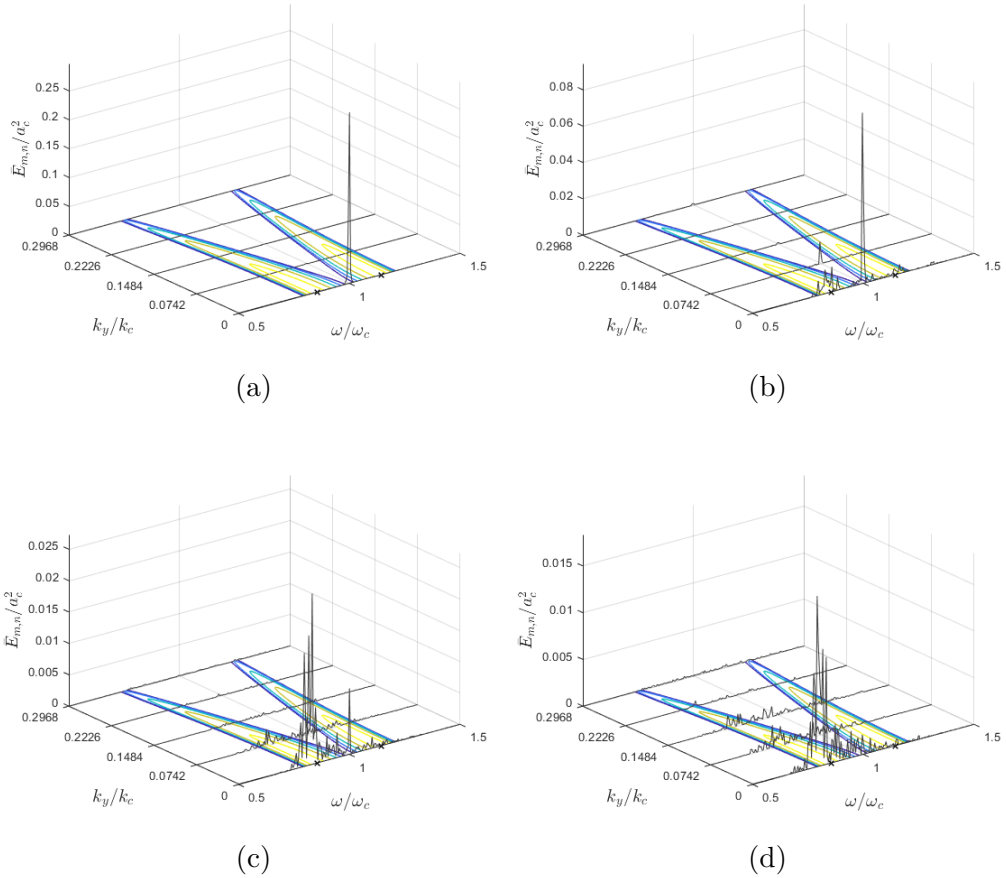

Figure 3.6: Energy distribution across longitudinal and transversal modes at (a): 10, (b): 80, (c): 120 and (d): 160 meters from the wave paddle. The instability region of the MNLS equation, calculated in section 2.5, is included for comparison.

this may be a combination of dissipation due to viscosity in the fluid and friction on the tank walls and air-liquid interface, as well as damping due to wave breaking if the waves become too steep. The precise conditions are complicated and nonuniform. It seems, however, that a good approximation is obtained with an exponentially decaying model. That is, we can estimate the energy evolution $\bar{E}(x)$ by a straight line, like we have done in figure (3.7) using the method of least squares. On linear axes this line corresponds to

$$10^{mx+b} = e^{\ln 10(mx+b)} = e^{mx \ln 10 + b \ln 10} = e^{b \ln 10} e^{mx \ln 10}, \tag{3.32}$$

with $m = -0.0017$ m^{-1} and $b = -0.2782$. That is, the total energy should behave somewhat according to

$$\bar{E} \propto e^{-0.0040x}. \tag{3.33}$$

According to equation (3.30) and (2.102), the wave envelope should in turn be proportional to the square root

$$B \propto e^{-0.0020x}. \tag{3.34}$$

For the moment, neither the NLS equation nor the MNLS equation includes this type of behaviour. A basic way to fix this is to simply include a linear term such as

$$\nu B, \tag{3.35}$$

with $\nu = 0.0020$ m^{-1} describing the intensity of the damping.

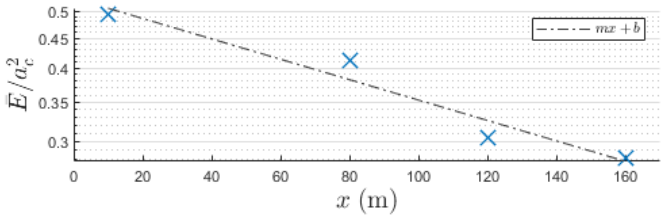

Figure 3.7: The total energy evolution can be approximated by a straight line according to the method of least squares. The rate of decay is determined by the slope m of this line.

CHAPTER 4

The numerical models and their implementation

4.1 The NLS scheme

The nonlinear Schrödinger equation

$$\frac{\partial B}{\partial x} + \frac{2k_c}{\omega_c}\frac{\partial B}{\partial t} + \frac{\mathrm{i}k_c}{\omega_c^2}\frac{\partial^2 B}{\partial t^2} - \frac{\mathrm{i}}{2k_c}\frac{\partial^2 B}{\partial y^2} + \mathrm{i}k_c^3|B|^2 B = 0 \tag{4.1}$$

consists almost entirely of linear terms. Such terms are exactly solvable with respect to the harmonic methods that we encountered in section 2.1. For this reason we may write (4.1) as

$$\frac{\partial B}{\partial x} + S_1 B + S_2 B = 0, \tag{4.2}$$

where the two operators S_1 and S_2 acting on B are given by

$$\begin{aligned} S_1 B &= \frac{2k_c}{\omega_c}\frac{\partial B}{\partial t} + \frac{\mathrm{i}k_c}{\omega_c^2}\frac{\partial^2 B}{\partial t^2} - \frac{\mathrm{i}}{2k_c}\frac{\partial^2 B}{\partial y^2}, \\ S_2 B &= \mathrm{i}k_c^3|B|^2 B. \end{aligned} \tag{4.3}$$

This operator splitting leads to the two sub-equations

$$\frac{\partial B_1}{\partial x} + \frac{2k_c}{\omega_c}\frac{\partial B_1}{\partial t} + \frac{\mathrm{i}k_c}{\omega_c^2}\frac{\partial^2 B_1}{\partial t^2} - \frac{\mathrm{i}}{2k_c}\frac{\partial^2 B_1}{\partial y^2} = 0, \tag{4.4a}$$

$$\frac{\partial B_2}{\partial x} + \mathrm{i}k_c^3|B_2|^2 B_2 = 0, \tag{4.4b}$$

which can be solved interchangeably according to the Lie scheme (2.36) or the Strang scheme (2.42), in order to achieve an approximate solution

to equation (4.1). Before getting into the details of the particular scheme, let us examine the solutions to (4.4a) and (4.4b) independently. With a periodic Dirichlet condition in time and a homogenous Neumann condition[1] in space, we can transform equation (4.4a) according to (2.11) and (2.22) respectively, resulting in

$$\frac{\mathrm{d}\widehat{B_1}_{m,n}}{\mathrm{d}x}+\frac{2k_c}{\omega_c}(-\mathrm{i}\omega_n)\widehat{B_1}_{m,n}+\frac{\mathrm{i}k_c}{\omega_c^2}(-\mathrm{i}\omega_n)^2\widehat{B_1}_{m,n}-\frac{\mathrm{i}}{2k_c}(-k_m^2)\widehat{B_1}_{m,n}=0, \quad (4.5)$$

for $m \in \mathbb{N}$ and $n \in \mathbb{Z}$. For every pair (k_m, ω_n) this is a linear, first order, homogenous ODE

$$\frac{\mathrm{d}\widehat{B_1}_{m,n}}{\mathrm{d}x} - \mathrm{i}\left(\frac{2k_c\omega_n}{\omega_c} + \frac{k_c\omega_n^2}{\omega_c^2} - \frac{k_m^2}{2k_c}\right)\widehat{B_1}_{m,n} = 0, \quad (4.6)$$

whose solution is given by

$$\widehat{B_1}_{m,n}(x) = \widehat{B_1}_{m,n}(x_0)e^{\mathrm{i}\left(\frac{2k_c\omega_n}{\omega_c}+\frac{k_c\omega_n^2}{\omega_c^2}-\frac{k_m^2}{2k_c}\right)(x-x_0)} \quad (4.7)$$

for $x \geq x_0$ and some appropriate initial condition $\widehat{B_1}_{m,n}(x_0)$. Equation (4.4b) can also be solved exactly since the absolute value of the solution remains unaffected with respect to the evolution variable;

$$|B_2(x,y,t)| = |B_2(x_0,y,t)| \quad \text{for all } x \geq x_0. \quad (4.8)$$

This allows us to consider (4.4b) as a linear, first order, homogenous ODE whose solution is given by

$$B_2(x,y,t) = B_2(x_0,y,t)e^{-\mathrm{i}k_c^3|B_2(x_0,y,t)|^2(x-x_0)}. \quad (4.9)$$

Before combining the above solutions in terms of a splitting scheme, we must discretize the independent variables x, y and t. The discretization of y and t depends on the number of modes $M \times N$ that we include in the numerical model, which due to the bandwidth constraint is limited by the requirement that

$$\frac{k_m}{k_c} < 1 \quad \text{and} \quad \frac{|\omega_n|}{\omega_c} < 1. \quad (4.10)$$

This ensures that there is no energy leakage[2] to arbitrarily high modes. Choosing M and N so that (4.10) is satisfied, we can place the computational

[1] A Dirichlet condition specifies the solution on the boundary of the domain, while a Neumann condition specifies its derivative there.

[2] A discussion on energy leakage in the three dimensional NLS equation can be found in [MY80].

grid according to

$$x_k = k\Delta x; \quad \Delta x = \frac{L_x}{K}; \quad k = 0, \ldots, K, \tag{4.11a}$$

$$y_i = (i + 1/2)\Delta y; \quad \Delta y = \frac{L_y}{M}; \quad i = 0, \ldots, M-1, \tag{4.11b}$$

$$t_j = j\Delta t; \quad \Delta t = \frac{T}{N}; \quad j = 0, \ldots, N-1, \tag{4.11c}$$

and write $\widehat{B_1}_{m,n}^{\,k}$ and ${B_2}_{i,j}^{k}$ in place of $\widehat{B_1}_{\,m,n}(x_k)$ and $B_2(x_k, y_i, t_j)$ respectively. It is clear that S_1 and S_2 do not commute since

$$S_1 S_2 B \neq S_2 S_1 B. \tag{4.12}$$

Let us therefore combine (4.7) and (4.9) according to the Strang scheme (2.42) so that we achieve a second order accurate solution to equation (4.1). Given an initial condition $\widehat{B}^0_{m,n} = \widehat{B}_{m,n}(x_0)$, this results in the iterative scheme

$$\begin{cases} \widehat{B_1}_{\,m,n}^{\,k+\frac{1}{2}} &= \widehat{B}^k_{m,n} e^{\mathrm{i}\left(\frac{2k_c\omega_n}{\omega_c} + \frac{k_c\omega_n^2}{\omega_c^2} - \frac{k_m^2}{2k_c}\right)\frac{\Delta x}{2}} \\ {B_2}_{i,j}^{\,k+1} &= {B_1}_{i,j}^{\,k+\frac{1}{2}} e^{-\mathrm{i}k_c^3\left|{B_1}_{i,j}^{\,k+\frac{1}{2}}\right|^2\Delta x} \\ \widehat{B}^{k+1}_{m,n} &= \widehat{B_2}_{\,m,n}^{\,k+1} e^{\mathrm{i}\left(\frac{2k_c\omega_n}{\omega_c} + \frac{k_c\omega_n^2}{\omega_c^2} - \frac{k_m^2}{2k_c}\right)\frac{\Delta x}{2}} \end{cases} \tag{4.13}$$

which can be stopped at any $k \leq K-1$. This allows us to analyse the evolution of a Stokes wave through the transform of the envelope $\widehat{B}^{k+1}_{m,n}$ or the transform of the surface elevation $\widehat{\eta}^{k+1}_{m,n}$ which is reconstructed from $B^{k+1}_{i,j}$. In chapter 5 we take on this latter approach.

4.2 The MNLS scheme

The modified nonlinear Schrödinger equation

$$\frac{\partial B}{\partial x} + \frac{2k_c}{\omega_c}\frac{\partial B}{\partial t} + \frac{\mathrm{i}k_c}{\omega_c^2}\frac{\partial^2 B}{\partial t^2} - \frac{\mathrm{i}}{2k_c}\frac{\partial^2 B}{\partial y^2} + \mathrm{i}k_c^3|B|^2 B$$

$$- \frac{1}{\omega_c k_c}\frac{\partial^3 B}{\partial t \partial y^2} - \frac{8k_c^3}{\omega_c}|B|^2\frac{\partial B}{\partial t} - \frac{2k_c^3}{\omega_c}B^2\frac{\partial B^*}{\partial t} - \frac{4\mathrm{i}k_c^3}{\omega_c^2}B\frac{\partial \bar{\phi}}{\partial t} = 0 \quad \text{at } z = 0 \tag{4.14}$$

contains information about the induced slow drift $\bar{\phi}$. This requires that we solve, in addition, the following BVP

$$\frac{\partial \bar{\phi}}{\partial z} = -k_c \frac{\partial |B|^2}{\partial t} \quad \text{at } z = 0 \tag{4.15}$$

$$\frac{4k_c^2}{\omega_c^2}\frac{\partial^2 \bar{\phi}}{\partial t^2} + \frac{\partial^2 \bar{\phi}}{\partial y^2} + \frac{\partial^2 \bar{\phi}}{\partial z^2} = 0 \quad \text{for } -h < z < 0 \tag{4.16}$$

$$\frac{\partial \bar{\phi}}{\partial z} = 0 \quad \text{at } z = -h. \tag{4.17}$$

Considering the fact that these equations are linear in $\bar{\phi}$, we should be able to do this with little effort using once again the transforms (2.11) and (2.22). With this procedure, equation (4.16) reduces to

$$\frac{4k_c^2}{\omega_c^2}(-\mathrm{i}\omega_n)^2 \widehat{\phi}_{m,n} + (-k_m^2)\widehat{\phi}_{m,n} + \frac{\partial^2 \widehat{\phi}_{m,n}}{\partial z^2} = 0 \quad \text{for } -h < z < 0, \tag{4.18}$$

which is a linear, second order, homogenous ODE

$$\frac{\partial^2 \widehat{\phi}_{m,n}}{\partial z^2} - \left(\frac{4k_c^2\omega_n^2}{\omega_c^2} + k_m^2\right)\widehat{\phi}_{m,n} = 0 \quad \text{for } -h < z < 0 \tag{4.19}$$

for $m = 0, \ldots, M-1$ and $n = -N/2, \ldots, N/2-1$. The general solution to this equation is given by

$$\widehat{\phi}_{m,n}(x,z) = c_{m,n}(x)e^{P_{m,n}z} + d_{m,n}(x)e^{-P_{m,n}z} \quad \text{for } -h < z < 0, \tag{4.20}$$

where

$$P_{m,n} = \sqrt{\frac{4k_c^2\omega_n^2}{\omega_c^2} + k_m^2} \tag{4.21}$$

and $c_{m,n}(x)$ and $d_{m,n}(x)$ are constants to be determined from the transformed boundary conditions

$$\begin{aligned} \frac{\partial \widehat{\phi}_{m,n}}{\partial z} &= -k_c(-\mathrm{i}\omega_n)\widehat{|B|^2}_{m,n} \quad \text{at } z = 0 \\ \frac{\partial \widehat{\phi}_{m,n}}{\partial z} &= 0 \quad \text{at } z = -h. \end{aligned} \tag{4.22}$$

Inserting (4.20) into the bottom condition we obtain

$$\widehat{\phi}_{m,n}(x,z) = 2d_{m,n}(x)e^{P_{m,n}h}\cosh\left(P_{m,n}(z+h)\right), \tag{4.23}$$

which in turn yields

$$2d_{m,n}(x)P_{m,n}e^{P_{m,n}h}\sinh\left(P_{m,n}h\right) = \mathrm{i}k_c\omega_n\widehat{|B|^2}_{m,n} \tag{4.24}$$

when inserted into the surface condition. If m and n are not both zero we find that

$$d_{m,n}(x) = \frac{\mathrm{i}k_c\omega_n e^{-P_{m,n}h}\widehat{|B|^2}_{m,n}}{2P_{m,n}\sinh\left(P_{m,n}h\right)}, \tag{4.25}$$

while equation (4.24) is automatically satisfied for any choice of $d_{0,0}$. Therefore let us choose $d_{0,0} = 0$ for simplicity such that

$$\widehat{\phi}_{m,n}(x,z) = \begin{cases} 0, & m = n = 0 \\ \frac{\mathrm{i}k_c\omega_n\widehat{|B|^2}_{m,n}\cosh\left(P_{m,n}(z+h)\right)}{P_{m,n}\sinh\left(P_{m,n}h\right)}, & \text{otherwise.} \end{cases} \tag{4.26}$$

If we multiply this by $-\mathrm{i}\omega_n$ we obtain the transform

$$\widehat{\frac{\partial\bar{\phi}}{\partial t}}_{m,n}(x,0) = \begin{cases} 0, & m = n = 0 \\ \frac{k_c\omega_n^2\widehat{|B|^2}_{m,n}\coth\left(P_{m,n}h\right)}{P_{m,n}}, & \text{otherwise} \end{cases} \tag{4.27}$$

of the desired quantity $\frac{\partial\bar{\phi}}{\partial t}\Big|_{z=0}$, which is readily obtained with inverse transforms in time and space.

In the previous section we saw how the linear terms and the nonlinear reaction term could be solved exactly when isolated against the evolution operator. Let us therefore split the MNLS equation into three parts such that (4.14) is written as

$$\frac{\partial B}{\partial x} + S_1B + S_2B + S_3B = 0, \tag{4.28}$$

where the three operators S_1, S_2 and S_3 acting on B are given by

$$\begin{aligned} S_1B &= \frac{2k_c}{\omega_c}\frac{\partial B}{\partial t} + \frac{\mathrm{i}k_c}{\omega_c^2}\frac{\partial^2 B}{\partial t^2} - \frac{\mathrm{i}}{2k_c}\frac{\partial^2 B}{\partial y^2} - \frac{1}{\omega_c k_c}\frac{\partial^3 B}{\partial t\partial y^2}, \\ S_2B &= \mathrm{i}k_c^3|B|^2B, \\ S_3B &= -\frac{8k_c^3}{\omega_c}|B|^2\frac{\partial B}{\partial t} - \frac{2k_c^3}{\omega_c}B^2\frac{\partial B^*}{\partial t} - \frac{4\mathrm{i}k_c^3}{\omega_c^2}B\frac{\partial\bar{\phi}}{\partial t}\Big|_{z=0}. \end{aligned} \tag{4.29}$$

The resulting three sub-equations are

$$\frac{\partial B_1}{\partial x} + \frac{2k_c}{\omega_c}\frac{\partial B_1}{\partial t} + \frac{\mathrm{i}k_c}{\omega_c^2}\frac{\partial^2 B_1}{\partial t^2} - \frac{\mathrm{i}}{2k_c}\frac{\partial^2 B_1}{\partial y^2} - \frac{1}{\omega_c k_c}\frac{\partial^3 B_1}{\partial t \partial y^2} = 0, \tag{4.30a}$$

$$\frac{\partial B_2}{\partial x} + \mathrm{i}k_c^3 |B_2|^2 B_2 = 0, \tag{4.30b}$$

$$\frac{\partial B_3}{\partial x} - \frac{8k_c^3}{\omega_c}|B_3|^2\frac{\partial B_3}{\partial t} - \frac{2k_c^3}{\omega_c}B_3^2\frac{\partial B_3^*}{\partial t} - \frac{4\mathrm{i}k_c^3}{\omega_c^2}B_3\frac{\partial \bar{\phi}}{\partial t}\bigg|_{z=0} = 0. \tag{4.30c}$$

We solve equation (4.30a) in the same way as equation (4.4a). Its solution in given in frequency-wavenumber space by

$$\widehat{B_1}_{\,m,n}(x) = \widehat{B_1}_{\,m,n}(x_0)e^{\mathrm{i}\left(\frac{2k_c\omega_n}{\omega_c} + \frac{k_c\omega_n^2}{\omega_c^2} - \frac{k_m^2}{2k_c} + \frac{\omega_n k_m^2}{\omega_c k_c}\right)(x-x_0)}, \tag{4.31}$$

while the solution to equation (4.30b) is given by (4.9) as before. The new challenge is to figure out how to solve equation (4.30c) which, by all accounts, is not exactly solvable. As suggested at the very end of section 2.2, we must resort to some numerical method that has at least the same order of accuracy as the splitting method itself. Since we will use the second order Strang scheme (2.42) to compose the solutions to the sub-equations (4.30a-4.30c), an easy, yet appropriate choice is the second order, explicit Runge-Kutta method (2.48). With the discretization (4.11a-4.11c) this implies that $B_3(x_{k+1}, y_i, t_j)$ is approximated by

$$B_3{}_{i,j}^{k+1} = B_3{}_{i,j}^{k} - \frac{1}{2}\Delta x(S_3 B_3{}_{i,j}^{k} + S_3(B_3{}_{i,j}^{k} - \Delta x S_3 B_3{}_{i,j}^{k})), \tag{4.32}$$

where $B_3{}_{i,j}^{k}$ is an initial condition on the interval $[x_k, x_{k+1}]$. This requires that we somehow replace the derivatives appearing in the operator

$$S_3 B_3{}_{i,j}^{k} = -\frac{8k_c^3}{\omega_c}|B_3{}_{i,j}^{k}|^2\frac{\partial B_3}{\partial t}_{i,j}^{k} - \frac{2k_c^3}{\omega_c}(B_3{}_{i,j}^{k})^2\frac{\partial B_3^*}{\partial t}_{i,j}^{k} - \frac{4\mathrm{i}k_c^3}{\omega_c^2}B_3{}_{i,j}^{k}\frac{\partial \bar{\phi}}{\partial t}\bigg|_{z=0}{}_{i,j}^{k}. \tag{4.33}$$

The standard way to do this is to once again resort to the theory of chapter 2.1. In particular, the identity (2.13) allows us to write

$$\frac{\widehat{\partial B_3}}{\partial t}_{m,n}^{k} = -\mathrm{i}\omega_n \widehat{B_3}_{m,n}^{k} \tag{4.34}$$

to which inverse transforms are applied in space and time to yield

$$\frac{\partial B_3}{\partial t}_{i,j}^{k} \quad \text{and} \quad \frac{\partial B_3^*}{\partial t}_{i,j}^{k} = \left(\frac{\partial B_3}{\partial t}_{i,j}^{k}\right)^*. \tag{4.35}$$

These quantities are calculated together with $\left.\frac{\partial\bar{\phi}}{\partial t}\right|_{z=0}{}^{k}_{i,j}$ from the initial condition at every iteration of the resulting operator splitting scheme

$$\begin{cases} \widehat{B_1}{}^{k+\frac{1}{2}}_{m,n} &= \widehat{B}^{k}_{m,n} e^{\mathrm{i}\left(\frac{2k_c\omega_n}{\omega_c}+\frac{k_c\omega_n^2}{\omega_c^2}-\frac{k_m^2}{2k_c}+\frac{\omega_n k_m^2}{\omega_c k_c}\right)\frac{\Delta x}{2}} \\ {B_2}^{k+\frac{1}{2}}_{i,j} &= {B_1}^{k+\frac{1}{2}}_{i,j} e^{-\mathrm{i}k_c^3\left|{B_1}^{k+\frac{1}{2}}_{i,j}\right|^2\frac{\Delta x}{2}} \\ {B_3}^{k+1}_{i,j} &= {B_2}^{k+\frac{1}{2}}_{i,j} - \frac{1}{2}\Delta x\Big(\tilde{S}_3 {B_2}^{k+\frac{1}{2}}_{i,j} + \tilde{S}_3\Big({B_2}^{k+\frac{1}{2}}_{i,j} - \Delta x\tilde{S}_3 {B_2}^{k+\frac{1}{2}}_{i,j}\Big)\Big) \\ {B_2}^{k+1}_{i,j} &= {B_3}^{k+1}_{i,j} e^{-\mathrm{i}k_c^3\left|{B_3}^{k+1}_{i,j}\right|^2\frac{\Delta x}{2}} \\ \widehat{B}^{k+1}_{m,n} &= \widehat{B_2}{}^{k+1}_{m,n} e^{\mathrm{i}\left(\frac{2k_c\omega_n}{\omega_c}+\frac{k_c\omega_n^2}{\omega_c^2}-\frac{k_m^2}{2k_c}+\frac{\omega_n k_m^2}{\omega_c k_c}\right)\frac{\Delta x}{2}}. \end{cases} \tag{4.36}$$

4.3 The model with damping

Both the NLS and MNLS equations conserve the total energy in the waves. In the real world, however, energy is lost in a multitude of ways, which was made clear in our analysis of the experimental data in chapter 3. As our goal is to investigate the effects of damping on three dimensional modulation of Stokes waves, we explain in the following how we can alter the conservative nature of the governing equations. In section 3.4 we found that the waves measured at Marintek were damped according to

$$B \propto e^{-\nu x} \tag{4.37}$$

where $\nu = 0.0020\ \mathrm{m}^{-1}$. It is well-known that the exponential function in (4.37) solves the equation

$$\frac{\partial B}{\partial x} + \nu B = 0, \tag{4.38}$$

so by adding a linear term such as νB to our governing equations, we should already be able to describe, in a simplified manner, the damping of waves. We picture that the parameter ν describes the combined effects of friction on the tank walls and air-water interface as well as viscosity in the water due to the water molecules themselves and the organic matter that builds up over time. This is readily accounted for in the splitting scheme above. We simply alter the exponent of the linear solution such that it reads

$$\widehat{B_1}_{m,n}(x) = \widehat{B_1}_{m,n}(x_0) e^{\mathrm{i}\left(\frac{2k_c\omega_n}{\omega_c}+\frac{k_c\omega_n^2}{\omega_c^2}-\frac{k_m^2}{2k_c}+\frac{\omega_n k_m^2}{\omega_c k_c}+\mathrm{i}\nu\right)(x-x_0)}. \tag{4.39}$$

Wave breaking on the other hand is a somewhat more complicated process that only happens in the areas where the waves are steep enough. For this reason we only want to add a breaking term when the local steepness $k_c|B|$ exceeds some predetermined threshold $k_c B^\star$. This can be achieved with the Heaviside step function, defined by

$$\mathrm{H}(x) = \begin{cases} 0, & x < 0 \\ 1, & x \geq 0. \end{cases} \tag{4.40}$$

Taking inspiration from [TD90], we introduce the term

$$\frac{k_c}{\tau} B\Big(\Big(\frac{|B|}{B^\star}\Big)^r - 1\Big)\mathrm{H}(|B| - B^\star) \tag{4.41}$$

where r and τ are constants that determine how fast the local amplitude $|B|$ decays towards the threshold $B^\star$. To get a better idea of the role of these parameters, let's look for the solution when the Heaviside step function outputs unity and the breaking term is isolated against the evolution operator

$$\frac{\partial B}{\partial x} + \frac{k_c}{\tau} B\Big(\Big(\frac{|B|}{B^\star}\Big)^r - 1\Big) = 0. \tag{4.42}$$

Assuming that $B = |B|e^{\mathrm{i}\theta}$, we obtain an equation that can be separated into its real and imaginary parts

$$\frac{\partial |B|}{\partial x} + \frac{k_c}{\tau}|B|\Big(\Big(\frac{|B|}{B^\star}\Big)^r - 1\Big) = 0, \qquad \frac{\partial \theta}{\partial x}|B| = 0. \tag{4.43}$$

The real part is effectively a separable ODE. We can therefore rearrange the terms and integrate with respect to x so that

$$\int \frac{d|B|}{|B|\Big(\Big(\frac{|B|}{B^\star}\Big)^r - 1\Big)} = -\frac{k_c}{\tau}\int dx. \tag{4.44}$$

With the substitution $u = \Big(\frac{|B|}{B^\star}\Big)^r - 1$, this simplifies to

$$\frac{1}{r}\int \frac{du}{u(u+1)} = -\frac{k_c x}{\tau} + c \tag{4.45}$$

where the integration constant c depends on y and t. We perform a partial fraction decomposition to the integrand and complete the integration so that

$$\frac{1}{r}\ln\Big(\frac{u}{u+1}\Big) = -\frac{k_c x}{\tau} + c \tag{4.46}$$

or equivalently

$$\frac{u}{u+1} = ce^{-\frac{rk_c x}{\tau}}. \tag{4.47}$$

Upon undoing the substitution and solving for the amplitude we then find that

$$|B(x,y,t)| = B^\star(1 - c(y,t)e^{-\frac{rk_c x}{\tau}})^{-\frac{1}{r}}, \tag{4.48}$$

which implies that the typical breaking event has a duration of $\frac{\tau}{rk_c}$. The constant c can be determined from the local amplitude when breaking starts at some x_0 such that

$$|B(x,y,t)| = B^\star\left(1 - \left(1 - \left(\frac{|B(x_0,y,t)|}{B^\star}\right)^{-r}\right)e^{-\frac{rk_c(x-x_0)}{\tau}}\right)^{-\frac{1}{r}}. \tag{4.49}$$

This solution is illustrated in figure 4.1 for $k_c = 2.9920\ \mathrm{m}^{-1}$, $r = 4$, $\tau = \frac{1}{8}$, $k_c B^\star = 0.25$ and $k_c|B| = 0.27$. It is seen that the breaking event transpires exponentially, but never past the threshold $B^\star$ which is indicated by the horizontal dashed line. The typical duration of a breaking event can be seen where the vertical dashed line meets the $x-$axis. As the solution to the imaginary part is constant with respect to x, the complete solution to equation (4.42) can be written

$$B(x,y,t) = B^\star\left(1 - \left(1 - \left(\frac{|B(x_0,y,t)|}{B^\star}\right)^{-r}\right)e^{-\frac{rk_c(x-x_0)}{\tau}}\right)^{-\frac{1}{r}} e^{\mathrm{i}\theta(x_0,y,t)}. \tag{4.50}$$

Since the breaking term (4.41) can be solved exactly when isolated against the evolution operator, we split the damped MNLS equation into four parts such that

$$\frac{\partial B}{\partial x} + S_1 B + S_2 B + S_3 B + S_4 B = 0. \tag{4.51}$$

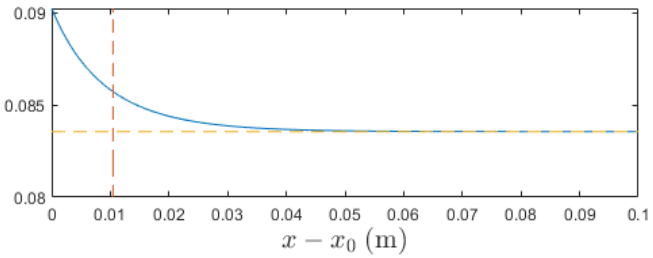

Figure 4.1: The local amplitude |B|: – is plotted for $k_c = 2.9920\ \mathrm{m}^{-1}$, $r = 4$, $\tau = \frac{1}{8}$, $k_c B^\star = 0.25$ and $k_c|B| = 0.27$. The typical duration of a breaking event $\frac{\tau}{rk_c}$: – – and the threshold $B^\star$: – – is included.

This time we let the operators S_1, S_2, S_3 and S_4 acting on B be defined by

$$\begin{aligned}
S_1 B &= \frac{2k_c}{\omega_c}\frac{\partial B}{\partial t} + \frac{\mathrm{i}k_c}{\omega_c^2}\frac{\partial^2 B}{\partial t^2} - \frac{\mathrm{i}}{2k_c}\frac{\partial^2 B}{\partial y^2} - \frac{1}{\omega_c k_c}\frac{\partial^3 B}{\partial t \partial y^2},\\
S_2 B &= \mathrm{i}k_c^3 |B|^2 B,\\
S_3 B &= \frac{k_c}{\tau} B\Big(\Big(\frac{|B|}{B^\star}\Big)^r - 1\Big)\mathrm{H}(|B| - B^\star),\\
S_4 B &= -\frac{8k_c^3}{\omega_c}|B|^2\frac{\partial B}{\partial t} - \frac{2k_c^3}{\omega_c}B^2\frac{\partial B^*}{\partial t} - \frac{4\mathrm{i}k_c^3}{\omega_c^2}B\frac{\partial \bar{\phi}}{\partial t}\Big|_{z=0},
\end{aligned} \tag{4.52}$$

so that the sub-equations that we solve read

$$\frac{\partial B_1}{\partial x} + \frac{2k_c}{\omega_c}\frac{\partial B_1}{\partial t} + \frac{\mathrm{i}k_c}{\omega_c^2}\frac{\partial^2 B_1}{\partial t^2} - \frac{\mathrm{i}}{2k_c}\frac{\partial^2 B_1}{\partial y^2} - \frac{1}{\omega_c k_c}\frac{\partial^3 B_1}{\partial t \partial y^2} = 0, \tag{4.53a}$$

$$\frac{\partial B_2}{\partial x} + \mathrm{i}k_c^3 |B_2|^2 B_2 = 0, \tag{4.53b}$$

$$\frac{\partial B_3}{\partial x} + \frac{k_c}{\tau} B_3\Big(\Big(\frac{|B_3|}{B^\star}\Big)^r - 1\Big)\mathrm{H}(|B_3| - B^\star) = 0, \tag{4.53c}$$

$$\frac{\partial B_4}{\partial x} - \frac{8k_c^3}{\omega_c}|B_4|^2\frac{\partial B_4}{\partial t} - \frac{2k_c^3}{\omega_c}B_4^2\frac{\partial B_4^*}{\partial t} - \frac{4\mathrm{i}k_c^3}{\omega_c^2}B_4\frac{\partial \bar{\phi}}{\partial t}\Big|_{z=0} = 0. \tag{4.53d}$$

After discretization of (4.50), the operator splitting scheme (4.36) can be adjusted to account for breaking. The result is

$$\begin{cases}
\widehat{B_1}_{m,n}^{k+\frac{1}{2}} &= \widehat{B}_{m,n}^{k} e^{\mathrm{i}\left(\frac{2k_c\omega_n}{\omega_c} + \frac{k_c\omega_n^2}{\omega_c^2} - \frac{k_m^2}{2k_c} + \frac{\omega_n k_m^2}{\omega_c k_c}\right)\frac{\Delta x}{2}}\\
{B_2}_{i,j}^{k+\frac{1}{2}} &= {B_1}_{i,j}^{k+\frac{1}{2}} e^{-\mathrm{i}k_c^3\left|{B_1}_{i,j}^{k+\frac{1}{2}}\right|^2\frac{\Delta x}{2}}\\
{B_3}_{i,j}^{k+\frac{1}{2}} &= B^\star\Big(1 - \Big(1 - \Big(\frac{|{B_2}_{i,j}^{k+\frac{1}{2}}|}{B^\star}\Big)^{-r}\Big)e^{-\frac{rk_c\Delta x}{2\tau}}\Big)^{-\frac{1}{r}} e^{\mathrm{i}\theta_{i,j}^{k+\frac{1}{2}}}, \quad \theta_{i,j}^{k+\frac{1}{2}} = \mathrm{phase}({B_2}_{i,j}^{k+\frac{1}{2}})\\
{B_4}_{i,j}^{k+1} &= {B_3}_{i,j}^{k+\frac{1}{2}} - \frac{1}{2}\Delta x\Big(\tilde{S}_4 {B_3}_{i,j}^{k+\frac{1}{2}} + \tilde{S}_4\Big({B_3}_{i,j}^{k+\frac{1}{2}} - \Delta x\tilde{S}_4 {B_3}_{i,j}^{k+\frac{1}{2}}\Big)\Big)\\
{B_3}_{i,j}^{k+1} &= B^\star\Big(1 - \Big(1 - \Big(\frac{|{B_4}_{i,j}^{k+1}|}{B^\star}\Big)^{-r}\Big)e^{-\frac{rk_c\Delta x}{2\tau}}\Big)^{-\frac{1}{r}} e^{\mathrm{i}\theta_{i,j}^{k+1}}, \quad \theta_{i,j}^{k+1} = \mathrm{phase}({B_4}_{i,j}^{k+1})\\
{B_2}_{i,j}^{k+1} &= {B_3}_{i,j}^{k+1} e^{-\mathrm{i}k_c^3\left|{B_3}_{i,j}^{k+1}\right|^2\frac{\Delta x}{2}}\\
\widehat{B}_{m,n}^{k+1} &= \widehat{B_2}_{m,n}^{k+1} e^{\mathrm{i}\left(\frac{2k_c\omega_n}{\omega_c} + \frac{k_c\omega_n^2}{\omega_c^2} - \frac{k_m^2}{2k_c} + \frac{\omega_n k_m^2}{\omega_c k_c}\right)\frac{\Delta x}{2}}
\end{cases} \tag{4.54}$$

where the third solution operator is replaced by the identity operator whenever the initial conditions satisfy

$$\left|{B_2}_{i,j}^{k+\frac{1}{2}}\right| < B^\star, \qquad \left|{B_4}_{i,j}^{k+1}\right| < B^\star. \tag{4.55}$$

CHAPTER 5

Simulation results

5.1 Verifying the implementation

There are several ways in which we can verify the implementation of the schemes (4.13) and (4.36). It is well known that both the NLS and MNLS equations conserve the energy when no damping is introduced and that they preserve the periodic uniform shape of an unperturbed Stokes wave. It is easy to check that the implementation indeed maintains these properties. A little bit of work is required, however, to show that the implementation is second order accurate. For this purpose, fix x and let $B_{i,j}^q$ denote the numerical approximation of $B(y_i, t_j)$ corresponding to a grid of width $\frac{\Delta x}{2^q}$. Do not confuse the superscript with the evolution index. We say that the numerical method is $p-$th order accurate if

$$B_{i,j}^q - B(y_i, t_j) = c\Big(\frac{\Delta x}{2^q}\Big)^p + \mathcal{O}((\Delta x)^{p+1}) \tag{5.1}$$

for some constant $c \in \mathbb{C}$ depending on the exact solution B. Consider the ratio of differences between approximations with consecutively smaller grid size

$$\frac{B_{i,j}^q - B_{i,j}^{q+1}}{B_{i,j}^{q+1} - B_{i,j}^{q+2}}. \tag{5.2}$$

After adding and subtracting the exact solution $B(y_i, t_j)$ in the numerator and denominator we can apply (5.1) to obtain

$$\frac{B_{i,j}^q - B_{i,j}^{q+1}}{B_{i,j}^{q+1} - B_{i,j}^{q+2}} = \frac{c\Big(\frac{\Delta x}{2^q}\Big)^p - c\Big(\frac{\Delta x}{2^{q+1}}\Big)^p + \mathcal{O}\Big(\Big(\frac{\Delta x}{2^q}\Big)^{p+1}\Big)}{c\Big(\frac{\Delta x}{2^{q+1}}\Big)^p - c\Big(\frac{\Delta x}{2^{q+2}}\Big)^p + \mathcal{O}\Big(\Big(\frac{\Delta x}{2^q}\Big)^{p+1}\Big)} = \frac{1 - 2^{-p} + \mathcal{O}\Big(\frac{\Delta x}{2^q}\Big)}{2^{-p} - 2^{-2p} + \mathcal{O}\Big(\frac{\Delta x}{2^q}\Big)}. \tag{5.3}$$

Upon performing the long division on the right and taking the square of the absolute value we get

$$\left| \frac{B_{i,j}^{q} - B_{i,j}^{q+1}}{B_{i,j}^{q+1} - B_{i,j}^{q+2}} \right|^2 = 2^{2p} + \mathcal{O}\Big(\frac{\Delta x}{2^q}\Big) \tag{5.4}$$

which can be summed over $i \in I = \{0, \ldots, M-1\}$ and $j \in J = \{0, \ldots, N-1\}$ such that

$$\sum_{i,j} \left| \frac{B_{i,j}^{q} - B_{i,j}^{q+1}}{B_{i,j}^{q+1} - B_{i,j}^{q+2}} \right|^2 = \left\| \frac{B^{q} - B^{q+1}}{B^{q+1} - B^{q+2}} \right\|_{l^2(I,J)}^2 = MN\Big(2^{2p} + \mathcal{O}\Big(\frac{\Delta x}{2^q}\Big)\Big). \tag{5.5}$$

The order of accuracy, also referred to as the convergence rate, should then be readily obtained from the base 2 logarithm

$$p = \log_2 \left(\frac{1}{\sqrt{MN}} \left\| \frac{B^{q} - B^{q+1}}{B^{q+1} - B^{q+2}} \right\|_{l^2(I,J)} \right) + \mathcal{O}\Big(\frac{\Delta x}{2^q}\Big). \tag{5.6}$$

It is clear from this expression that the estimate of p is improved if we shrink the width of the grid $\frac{\Delta x}{2^q}$. It is therefore best that we compute (5.6) for multiple values of q.

We intend to use the NLS and MNLS equations to study the evolution of a Stokes wave with steepness $\varepsilon = a_c k_c = 0.1$. The wavenumber is chosen so that the ratio $\Delta\mu = \frac{\Delta k}{k_c} = \frac{\pi}{k_c L_y} = 0.1$. We perturb the Stokes wave randomly on 128 sidebands inside the square determined by $n = -21, -20, \ldots, 21$ and $m = 0, 1, 2$. This ensures that some of the perturbations lie within the unstable regions (2.1a-2.1b) and that energy is transfered to transversal modes as the waves propagate along the tank. The analytically most unstable sidebands are not perturbed. With this initialization of the program, we run the conservative schemes (4.13) and (4.36) for seven different discretizations $\frac{\Delta x}{2^q}$ where $\Delta x = 0.5$ and $q = 0, \ldots, 6$. The corresponding numerical solutions are stored at $x = 70$ m and we compute thereafter five consecutive estimates for the accuracy p. The results are presented in table 5.1. Both schemes show second order accuracy as the grid size progressively gets smaller, which suggests that the implementation is correct. It is evident that, in order to obtain a stable and satisfactory numerical solution, we should at least ensure that $\Delta x = \frac{0.5}{2^3} = 0.0625$. In the upcoming simulations, we let $\Delta x = 0.05$. With this choice of Δx we are confident that the numerical solution yields reliable insight about the evolution of a Stokes wave. The script of the program, as implemented in MATLAB, can be found in the appendix.

q	p_{NLS}	p_{MNLS}
0	8.774433215743645	NaN
1	2.317779495134089	2.154207330430582
2	2.045860210138446	2.024248251207924
3	2.010074151045264	2.007276316830951
4	2.002422784270935	2.003598848424581

Table 5.1: The convergence rate p is estimated for the implementation of the NLS and MNLS schemes at $x = 70$ m with $\Delta x = 0.5$.

5.2 The evolution of a Stokes wave

The conservative model

We let the randomly perturbed Stokes wave that we introduced in the previous section propagate along a tank, such as the one in figure 3.1, without the influence of damping. The evolution, according to the MNLS equation, is presented in figure (5.1). The energy distribution across longitudinal and transversal modes can be seen at (a): 0, (b): 40, (c): 80, (d): 120, (e) 160 and (f): 200 meters from the wave paddle. The nonlinear narrow-banded modulations that initiate the energy transfer between modes begin shortly after the waves leave the wave paddle. At this moment the carrier represents the most energetic frequency component, which shall be denoted hereon as the peak frequency ω_{peak}. Energy is transferred from the peak to both longitudinal and transversal modes as the waves propagate along the tank. In fact, the rate of energy transfer from the peak ω_{peak} increases during this initial modulation stage. This observation can be made from figure 5.2a where the total energy and the energy evolution of the peak is indicated by the red dash-dotted line and blue solid line respectively. At 80 meters from the wave paddle the peak has lost almost 90 percent of its energy to adjacent sidebands. Although many of the lower sidebands grow past the upper, the mean frequency

$$\omega_{\text{mean}} = \frac{1}{\bar{E}} \sum_{n=0}^{N/2-1} \omega_n (2 - \delta_{0,n}) \sum_{m=0}^{M-1} \bar{E}_{m,n} \tag{5.7}$$

is upshifted, as we can see from the red dash-dotted line in figure 5.2b. This is indicative of the emergence of a long tail of upper sidebands which becomes more prominent as the waves continue to propagate. Figure 5.2b also shows the frequency evolution of the peak ω_{peak} through the blue solid line. The sudden jump at $x = 82.1$ m indicates that one of the

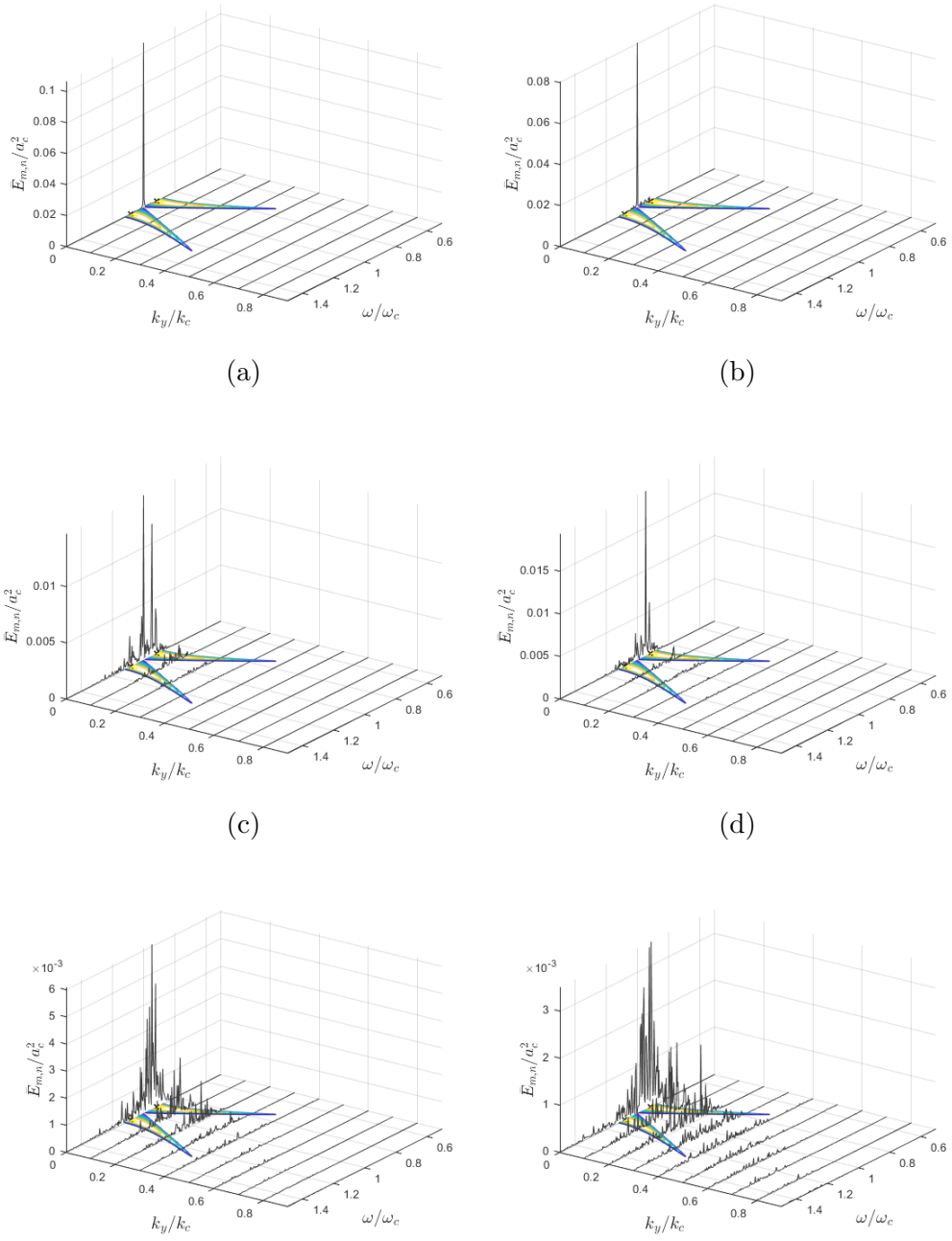

Figure 5.1: Energy distribution across longitudinal and transversal modes according to the conservative MNLS equation at (a): 0, (b): 40, (c): 80, (d): 120, (e): 160 and (f): 200 meters from the wave paddle. The corresponding instability region, calculated in section 2.5, is included for reference.

unstable lower sidebands eventually grows past the carrier and that the peak is downshifted. From figure 5.2a we see that this sideband continues to grow until it reaches a maximum at $x = 120$ m. From this point on the transversal modulation becomes much more perceptible as the energy is spread over a large number of sidebands. The asymmetrical shape of the energy distribution persists nonetheless as the mean ω_{mean} stabilizes at a frequency slightly larger than the characteristic frequency ω_c and the peak ω_{peak} oscillates between neighboring lower sidebands.

The conservative evolution of the randomly perturbed Stokes wave, according to the NLS equation, is included in figure 5.3. In the beginning stages of propagation, the modulation of the carrier is qualitatively the same as before. Energy is lost to the sidebands at an increasing rate and the peak frequency ω_{peak} remains unchanged for over 80 meters. When the downshift finally happens at $x = 89.4$ m it is, however, not permanent. The many subsequent jumps testify that the peak frequency ω_{peak} is no longer well defined. In addition, the mean frequency ω_{mean} does not at any point significantly shift away from the characteristic frequency ω_c. These two observations suggest that the energy is smeared across a large number of unstable sidebands and that the energy distribution is more or less symmetric about the characteristic frequency. For this reason, the NLS equation is not particularly suited as a model for permanent frequency downshift. Similar observations have been made by many before us. We therefore do not see any reason as to why we should continue to use the NLS equation. In the upcoming discussion we therefore confine ourselves to the application of the MNLS equation.

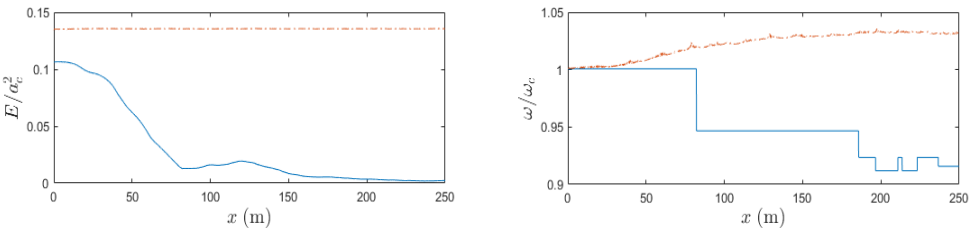

(a) (b)

Figure 5.2: The conservative evolution of a Stokes wave according to the MNLS equation. (a): The total energy: – · – and the energy in the peak frequency: –. (b): The peak frequency ω_{peak}: – and the mean frequency ω_{mean}: – · –.

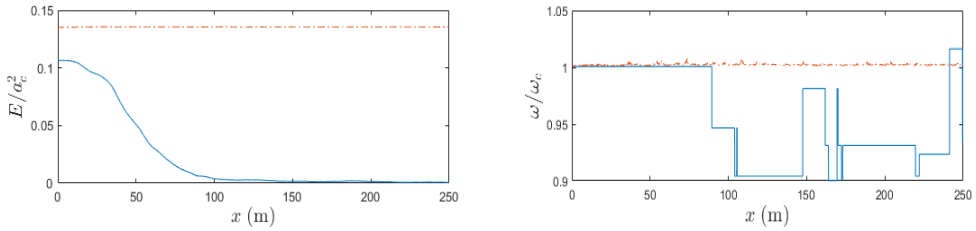

(a) (b)

Figure 5.3: The conservative evolution of a Stokes wave according to the NLS equation. (a): The total energy: – · – and the energy in the peak frequency: –. (b): The peak frequency ω_{peak}: – and the mean frequency ω_{mean}: – · –.

The impact of viscous damping

The above results are in accordance with the findings of [TD97]. They were the first to show numerically using the broader bandwidth nonlinear Schrödinger (BMNLS) equation that, unlike the two dimensional evolution of Stokes waves, three dimensional evolution does not require damping in order to produce a permanent downshift of the peak ω_{peak}. It is nonetheless interesting to investigate what the effects of damping can be. We therefore let the randomly perturbed Stokes wave propagate according to the viscously damped MNLS equation with $\nu = 0.0005$ m^{-1} and $\nu = 0.001$ m^{-1}. The evolution is presented in figures 5.4a-5.4b and 5.4c-5.4d respectively. It is readily compared with the conservative evolution which is indicated in the background. The energy evolution of the peak is qualitatively the same as before. This time, however, energy is not solely transferred to longitudinal and transversal modes, but also to the immediate surroundings. The energy evolution of the five smallest transverse modes is depicted in figure 5.5 together with the total energy for $\nu = 0.0005$ m^{-1}. It is evident that as the waves propagate along the tank, the viscous dissipation of energy slows down the emergence of each and every one of these modes. We note in this context that the mean ω_{mean} evolves in essentially the same way as before. The downshift of the peak ω_{peak} is however noticeably delayed and is witnessed at $x = 84.35$ m and $x = 87.7$ m for $\nu = 0.0005$ m^{-1} and $\nu = 0.001$ m^{-1} respectively. Still it is the same unstable lower sideband that becomes dominant for both values of the viscosity parameter ν. The oscillation of the peak ω_{peak} that was observed between neighboring lower sidebands at the end of the tank in the conservative evolution is completely gone.

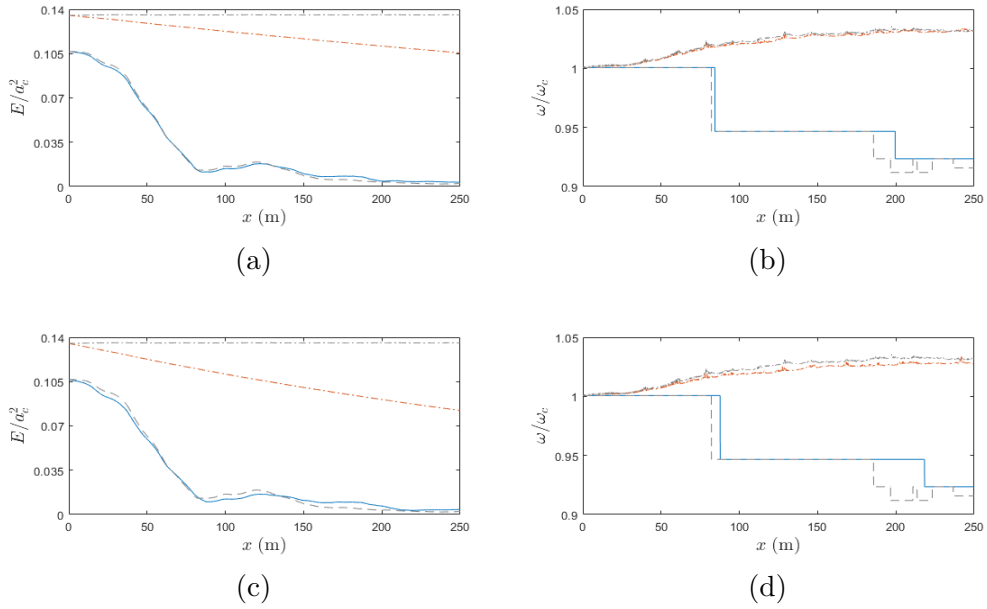

Figure 5.4: The evolution of a Stokes wave subjected to viscous damping. (a-b): $\nu = 0.0005$ m^{-1}. (c-d): $\nu = 0.0010$ m^{-1}. The conservative results: $--$ are included for reference. See caption of figure 5.2 for line styles.

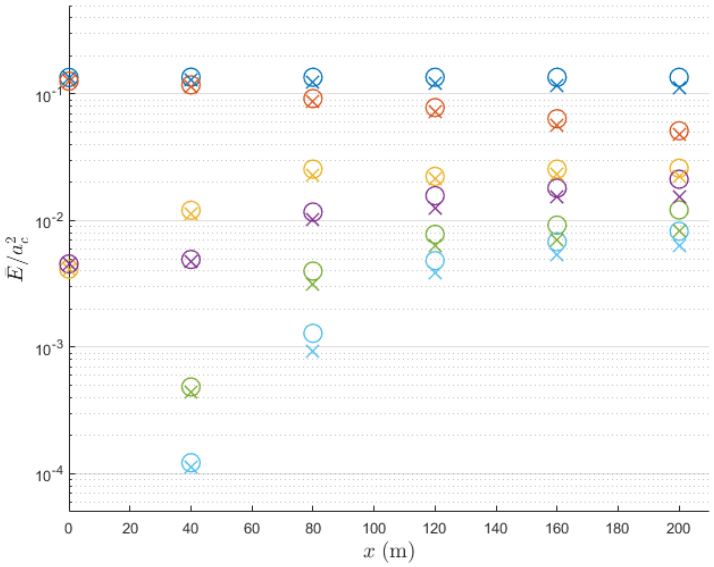

Figure 5.5: The energy evolution of the five smallest transversal modes according to the conservative: ◯ and viscous: × model. The total energy: blue, and the energy in k_0: red, k_1: yellow, k_2: purple, k_3: green and k_4: light blue, is plotted for $\nu = 0.0005$ m^{-1}.

The impact of wave breaking

We subject the randomly perturbed Stokes wave to damping through wave breaking, where the typical duration of a breaking event $\frac{\tau}{rk_c}$ is determined by $r = 4$ and $\tau = \frac{1}{8}$. The evolution corresponding to the two thresholds $k_cB^\star = 0.3$ and $k_cB^\star = 0.25$ can be seen in figures 5.6a-5.6b and 5.6c-5.6d respectively. Throughout the initial stages of propagation, the nonlinear modulation has yet to raise the steepness ε past the limiting threshold. The first signs of breaking can be seen, for both values of the threshold, from the sudden decrease of total energy at approximately 40 meters form the wave paddle. From hereon, it seems that the sidebands are damped selectively as the upshift of the mean ω_{mean} is strongly opposed even though the loss of total energy is small. This suggests that the long tail of upper sidebands, that results from the nonlinear modulation of the wave train, goes to zero faster than before. The selective damping of upper sidebands is emphasized in figure 5.7 where the energy evolution of the five smallest transversal modes can be seen together with the total energy for $k_cB^\star = 0.25$. The two smallest components k_0 and k_1 are barely affected by the breaking term. The consecutive modes are, however, significantly damped as the waves propagate along the tank. According to [TD90], who investigated the impact of modulation and breaking on frequency downshift in two dimensional wave trains, this feature is due to "...the tendency towards spatial localization of the part of the wavetrain contributing to the upper sidebands". Their assertion is supported by the experimental results of [Mel83]. The accelerated downshift of the peak ω_{peak}, which is seen at $x = 80.8$ m and $x = 80.25$ m for $k_cB^\star = 0.3$ and $k_cB^\star = 0.25$ respectively, is also in contrast to the results obtained from the viscous model. However, we have found that if we let the threshold $k_cB^\star$ be small enough, the delayed downshift recurs. We verify on the other hand that the specific choice of values for the parameters r and τ are insignificant for the results that we obtain. This is in agreement with the findings of [TD90].

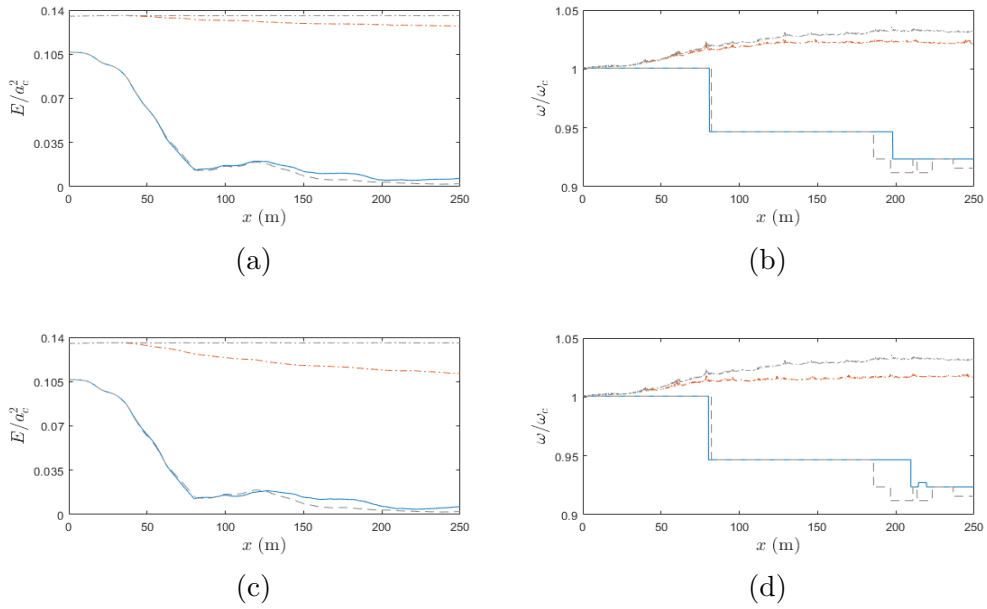

Figure 5.6: The evolution of a Stokes wave subjected to breaking. (a-b): $k_cB^\star = 0.3$. (c-d): $k_cB^\star = 0.25$. The conservative results: $--$ are included for reference. See caption of figure 5.2 for line styles.

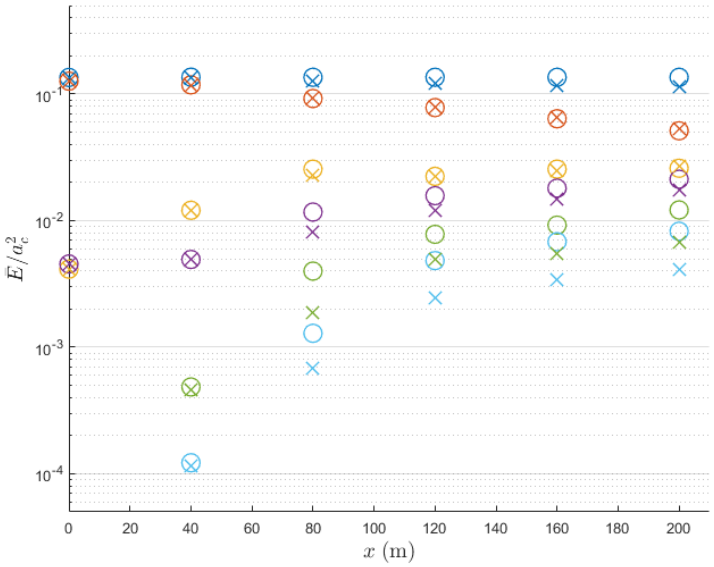

Figure 5.7: The energy evolution of the five smallest transversal modes according to the conservative: ◯ and wave-broken: × model. The total energy: blue, and the energy in k_0: red, k_1: yellow, k_2: purple, k_3: green and k_4: light blue, is plotted for $k_cB^\star = 0.25$.

CHAPTER 6

Concluding remarks

We have shown, using the modified nonlinear Schrödinger equation, that different types of damping can influence the frequency downshift of a three dimensional wave train. We have seen that viscous damping can postpone the downshift, while careful wave breaking may accelerate or expedite the downshift. We have also seen that while all modes are damped in the viscous model, the breaking model damps sidebands selectively. This extends the observations of [TD90] to three dimensions.

The present conclusions are drawn from the observations of only one randomly perturbed Stokes wave. In order to generalize these observations to the general Stokes wave, we would need to perform a thorough statistical analysis with ensemble averaging. This may be an interesting continuation of the present thesis.

Appendices

APPENDIX A

The MATLAB code

Listings

Listing A.1: Implementation of the growth rates, the MNLS scheme and the corresponding accuracy test

```
1  clc; clear;
2
3  %% variables that stay constant
4  m = 42;
5  Ly = 10.5;
6  dky = pi/Ly;
7  ky = (0:m-1)*dky;
8  n = 4000;
9  T = 300;
10 dt = T/n;
```

```
11 dw = 2*pi/T;
12 w = (-n/2:n/2-1)*dw;
13 g  = 9.82;
14 h = 5;
15
16 %% parameters that can be varied
17
18 %steepness and transverse modulation
19 epsilon = 0.1;
20 dmu = 0.1;
21
22 %characteristic variables, group velocity and
      nondimensional depth
23 kc = dky/dmu;
24 ac = epsilon/kc;
25 wc = sqrt(g*kc);
26 Cg = g/(2*wc);
27 d = kc*h;
28
29 %% Analytical region of unstable perturbations
30
31 [omega,mu] = meshgrid(-0.8*wc:0.01:0.8*wc,0:0.01:0.95*kc);
32 Q = kc/wc^2*omega.^2-1/(2*kc)*mu.^2;
33 R = sqrt(4*kc^2/wc^2*omega.^2+mu.^2);
34
35 %analytical region of unstable perturbations - NLS equation
36 growth_rate_NLS = imag(sqrt(Q.*(Q-2*kc*epsilon^2)));
37
38 %hyperbola of maximum growth rate - NLS equation
39 max_growth_rate_NLS = real(sqrt(2*kc^2/wc^2*omega(1,:)
      .^2-2*kc^2*epsilon^2));
40
41 %analytical region of unstable perturbations - MNLS
      equation
42 growth_rate_MNLS = imag(sqrt(Q.*(Q-2*kc*epsilon^2+8*kc^2*
      epsilon^2./(wc^2*R).*coth(R*h).*omega.^2)+4*kc^2*epsilon
      ^4/wc^2*omega.^2));
43
44 %points of maximum growth rate - MNLS equation
45 omega1 = wc*epsilon*(-3/2*epsilon+1/2*sqrt(epsilon^2+4));
46 omega2 = wc*epsilon*(3/2*epsilon-1/2*sqrt(epsilon^2+4));
```

```
47
48 %% setup of program and initial condition
49
50 %bandwidth constraint on envelope
51 sim_idx_w = find(-wc<w & w<wc);
52 sim_idx_w = [sim_idx_w(1)-1,sim_idx_w];
53 sim_idx_ky = find(ky<kc);
54
55 %frequency and wavenumber mesh
56 [W,KY] = meshgrid(w(1,sim_idx_w),ky(sim_idx_ky));
57 [M,N] = size(W); %ensure that N is even
58
59 %constants appearing in the NLS and MNLS equations
60 c1 = 2*kc/wc;
61 c2 = kc/wc^2;
62 c3 = -1/(2*kc);
63 c4 = kc^3;
64 c5 = 1/(wc*kc);
65
66 %constants appearing in the solution for the induced slow
      drift
67 P = sqrt(4*kc^2/wc^2*W.^2+KY.^2);
68 const = kc*W.^2./P.*coth(P*h);
69 const(1,N/2+1) = 0;
70
71 %Stokes wave initial condition
72 BStilde = zeros(M,N);
73 BStilde(1,N/2+1) = ac;
74
75 %perturbed Stokes wave initial condition
76 B0tilde = zeros(M,N);
77 B0tilde(1:ceil(M/4),floor(11*N/24)+1:floor(13*N/24)) = ac*
      epsilon*complex(rand(ceil(M/4),length(floor(11*N/24)+1:
      floor(13*N/24)))-0.5,rand(ceil(M/4),length(floor(11*N
      /24)+1:floor(13*N/24)))-0.5);
78 B0tilde(1,N/2+1) = ac;
79
80 %initial envelope
81 B0 = [B0tilde;complex(zeros(m-M,N))];
82 B0 = [complex(zeros(m,(n-N)/2)),B0,complex(zeros(m,(n-N)/2)
      )];
```

```
83  B0 = sqrt(M)*[B0(1,:);1/sqrt(2)*B0(2:end,:)];
84  B0 = fft(idct(ifftshift(B0,2),'Type',2).').';
85
86  %initial temporal mesh
87  T0 = repelem(0:dt:T-dt,m,1);
88
89  %initial surface elevation
90  Z0 = real(B0.*(1-3/8*kc^2*B0.^2).*exp(1i*(0*kc-wc*T0))+kc
        /2*B0.^2.*exp(2i*(0*kc-wc*T0))+3/8*kc^2*B0.^3.*exp(3i
        *(0*kc-wc*T0)));
91
92  %transform
93  Z0tilde = fftshift(ifft(dct(Z0,'Type',2).').',2);
94  Z0tilde = 1/sqrt(m)*[Z0tilde(1,:);sqrt(2)*Z0tilde(2:end,:)
        ];
95
96  %initial energy
97  H0 = abs(Z0tilde).^2;
98  E0 = 1/2*sum(sum([2*H0(1,:);H0(2:end,:)])); %total energy
99  EK0 = 1/2*sum([2*H0(1,:);H0(2:M,:)].').'; %energy in each
        transversal mode
100
101 %the energy is used as a probability density function
102 HOS0 = [H0(:,n/2+1),2*H0(:,n/2+2:end)];
103 PDF0 = 1/sum(sum([2*HOS0(1,:);HOS0(2:end,:)]))*[2*HOS0(1,:)
        ;HOS0(2:end,:)];
104
105 %initial nondimensional bandwidth
106 Delta_w0 = sqrt(sum(PDF0)*(w(1,n/2+1:end).'-wc).^2)/wc;
107 Delta_k0 = sqrt(sum(PDF0.')*(ky.').^2)/kc;
108
109 %initial peak frequency and spectral mean
110 peak0 = max(max(PDF0));
111 [peak_idx_ky0,peak_idx_w0] = find(PDF0==peak0);
112 kyp0 = ky(peak_idx_ky0);
113 wp0 = w(n/2+peak_idx_w0);
114 wm0 = sum(PDF0)*w(1,n/2+1:end).';
115
116 %% This code-section solves the MNLS-equation in space.
117
118 dx = 0.05;
```

```
119 Lx = 250;
120 K = Lx/dx;
121
122 %viscous damping parameter
123 nu = 0.0005;
124
125 %wave breaking parameters - the results are insensitive to
       variations in r and tau
126 tau = 1/8;
127 r = 4;
128 B_critical = 0.25/kc;
129 WB = exp(-r*kc/tau*dx/2);
130
131 %store the peak frequency, spectral mean and total energy
       at every x_k
132 PEAK = [[wp0;kyp0;1/2*peak0*sum(sum([2*HOS0(1,:);HOS0(2:end
       ,:)]))],zeros(3,K)];
133 MEAN = [wm0,zeros(1,K)];
134 ENERGY = [E0,zeros(1,K)];
135
136 %store the energy in each transversal wavenumber every 40 m
137 EK = [EK0,zeros(M,5)];
138 count=0;
139
140 %linear solution - the damping term in the exponent can be
       removed for
141 %conservative computations or computations with wave
       breaking
142 LS = exp(1i*(c1*W+c2*W.^2+c3*KY.^2+c5*W.*KY.^2+1i*nu)*dx/2)
       ;
143
144 %MULTI-COMPONENT OPERATOR SPLITTING - STRANG SYMMETRIZED
       SCHEME
145 Btilde = B0tilde;
146 for k = 0:K-1
147 %solve linear problem on (xk,xk+1/2)
148 Btilde = Btilde.*LS;
149 Btilde = sqrt(M)*[Btilde(1,:);1/sqrt(2)*Btilde(2:end,:)];
150 B = fft(idct(ifftshift(Btilde,2),'Type',2).').';
151
152 %solve second order nonlinear problem on (xk,xk+1/2)
```

```
153 B = B.*exp(-1i*c4*abs(B).^2*dx/2);
154
155 %solve the breaking term on (xk,xk+1/2)
156 breaking_idx = abs(B)>=B_critical;
157 B(breaking_idx) = B_critical*(1-(1-(abs(B(breaking_idx))/
       B_critical).^(-r))*WB).^(-1/r).*exp(1i*angle(B(
       breaking_idx)));
158
159 %solve third order nonlinear problem on (xk,xk+1)
160 SB = S(B,W,const,kc,wc);
161 B = B - 1/2*dx*(SB+S(B-dx*SB,W,const,kc,wc)); %explicit
       Runge-Kutta method
162
163 %solve the breaking term on (xk+1/2,xk+1)
164 breaking_idx = abs(B)>=B_critical;
165 B(breaking_idx) = B_critical*(1-(1-(abs(B(breaking_idx))/
       B_critical).^(-r))*WB).^(-1/r).*exp(1i*angle(B(
       breaking_idx)));
166
167 %solve second order nonlinear problem on (xk+1/2,xk+1)
168 B = B.*exp(-1i*c4*abs(B).^2*dx/2);
169
170 %solve linear problem on (xk+1/2,xk+1)
171 Btilde = fftshift(ifft(dct(B,'Type',2).',2);
172 Btilde = 1/sqrt(M)*[Btilde(1,:);sqrt(2)*Btilde(2:end,:)];
173 Btilde = Btilde.*LS;
174
175 %break if the scheme is unstable
176 if sum(sum(isnan(Btilde))) > 0
177     break;
178 end
179
180 %interpolation to account for the higher frequency content
       of the surface elevation
181 B = [complex(zeros(m,(n-N)/2)),[Btilde;complex(zeros(m-M,N)
       )],complex(zeros(m,(n-N)/2))];
182 B = sqrt(M)*[B(1,:);1/sqrt(2)*B(2:end,:)];
183 B = fft(idct(ifftshift(B,2),'Type',2).').';
184
185 %temporal mesh varies according to the group velocity
186 TK = repelem((k+1)*dx/Cg:dt:(k+1)*dx/Cg+T-dt,m,1);
```

```
187
188 %reconstruction
189 Z = real(B.*(1-3/8*kc^2*B.^2).*exp(1i*(kc*(k+1)*dx-wc*TK))+
    kc/2*B.^2.*exp(2i*(kc*(k+1)*dx-wc*TK))+3/8*kc^2*B.^3.*
    exp(3i*(kc*(k+1)*dx-wc*TK)));
190
191 %transform
192 Ztilde = fftshift(ifft(dct(Z,'Type',2).').',2);
193 Ztilde = 1/sqrt(m)*[Ztilde(1,:);sqrt(2)*Ztilde(2:end,:)];
194
195 %energy
196 H = abs(Ztilde).^2;
197 ENERGY(1,k+2) = 1/2*sum(sum([2*H(1,:);H(2:end,:)]));
198
199 %the energy in each transversal mode is stored every 40 m
200 if mod((k+1)*dx,40)==0
201     EK(:,count+2) = 1/2*sum([2*H(1,:);H(2:M,:)].').';
202     count=count+1;
203 end
204
205 %the energy is used as a probability density function
206 HOS = [H(:,n/2+1),2*H(:,n/2+2:end)];
207 PDF = 1/sum(sum([2*HOS(1,:);HOS(2:end,:)]))*[2*HOS(1,:);HOS
    (2:end,:)];
208
209 %dimensional bandwidth
210 Delta_w = sqrt(sum(PDF)*(w(1,n/2+1:end).'-wc).^2);
211 Delta_k = sqrt(sum(PDF.')*(ky.').^2);
212
213 %peak frequency and spectral mean
214 peak = max(max(PDF));
215 [peak_idx_ky,peak_idx_w] = find(PDF==peak);
216 PEAK(:,k+2) = [w(n/2+peak_idx_w);ky(peak_idx_ky);1/2*peak*
    sum(sum([2*HOS(1,:);HOS(2:end,:)]))];
217 MEAN(1,k+2) = sum(PDF)*w(1,n/2+1:end).';
218
219 end
220
221 %% Convergence-rate test for the MNLS equation
222
223 Lx = 70; %compare solutions at this value of x
```

```
224 U2 = zeros(M,N,7); %store consecutive solutions
225
226 for i=1:size(U2,3)
227
228 %halve the step-size in each iteration
229 dx = 0.5*(1/2)^(i-1);
230 K = Lx/dx;
231
232 %linear solution
233 LS = exp(1i*(c1*W+c2*W.^2+c3*KY.^2+c5*W.*KY.^2)*dx/2);
234
235 %MULTI-COMPONENT OPERATOR SPLITTING - STRANG SYMMETRIZED
       SCHEME
236 Btilde = B0tilde;
237 for k = 0:K-1
238 %solve linear problem on (xk,xk+1/2)
239 Btilde = Btilde.*LS;
240 Btilde = sqrt(M)*[Btilde(1,:);1/sqrt(2)*Btilde(2:end,:)];
241 B = fft(idct(ifftshift(Btilde,2),'Type',2).').';
242
243 %solve second order nonlinear problem on (xk,xk+1/2)
244 B = B.*exp(-1i*c4*abs(B).^2*dx/2);
245
246 %solve third order nonlinear problem on (xk,xk+1)
247 SB = S(B,W,const,kc,wc);
248 B = B - 1/2*dx*(SB+S(B-dx*SB,W,const,kc,wc));
249
250 %solve second order nonlinear problem on (xk+1/2,xk+1)
251 B = B.*exp(-1i*c4*abs(B).^2*dx/2);
252
253 %solve linear problem on (xk+1/2,xk+1)
254 Btilde = fftshift(ifft(dct(B,'Type',2).').',2);
255 Btilde = 1/sqrt(M)*[Btilde(1,:);sqrt(2)*Btilde(2:end,:)];
256 Btilde = Btilde.*LS;
257 end
258 Btilde = sqrt(M)*[Btilde(1,:);1/sqrt(2)*Btilde(2:end,:)];
259 B = fft(idct(ifftshift(Btilde,2),'Type',2).').';
260
261 U2(:,:,i) = B;
262 end
263
```

```
264 %vector containing the l2-norm of the ratio of differences
       between consecutive approximations
265 L2 = zeros(1,size(U2,3)-2);
266 for q=1:size(U2,3)-2
267     L2(q)=sqrt(sum(sum(abs((U2(:,:,q)-U2(:,:,q+1))./(U2
           (:,:,q+1)-U2(:,:,q+2))).^2)));
268 end
269
270 %estimate of the convergence rate p
271 log2([1/sqrt(M*N)*L2(1),1/sqrt(M*N)*L2(2),1/sqrt(M*N)*L2(3)
       ,1/sqrt(M*N)*L2(4),1/sqrt(M*N)*L2(5)])
```

Listing A.2: Implementation of the nonlinear operator (4.33) in the MNLS equation

```
1  function [SB] = S(B,W,const,kc,wc)
2
3  dphi_dt_tilde = const.*fftshift(ifft(dct(abs(B).^2,'Type'
       ,2).').',2);
4  dphi_dt = fft(idct(ifftshift(dphi_dt_tilde,2),'Type',2).')
       .';
5
6  dB_dt_tilde = -1i*W.*fftshift(ifft(dct(B,'Type',2).').',2);
7  dB_dt = fft(idct(ifftshift(dB_dt_tilde,2),'Type',2).').';
8
9  dBc_dt = conj(dB_dt);
10
11 SB = -8*kc^3/wc*abs(B).^2.*dB_dt-2*kc^3/wc*B.^2.*dBc_dt-4i*
       kc^3/wc^2*B.*dphi_dt;
12
13 end
```

Bibliography

[BF67] Benjamin, T. B. and Feir, J. E. 'The disintegration of wave trains on deep water Part 1. Theory'. eng. In: *Journal of fluid mechanics* vol. 27, no. 3 (1967), pp. 417–430.

[Fen85] Fenton, J. D. 'A fifth-order Stokes theory for steady waves'. eng. In: *Journal of Waterway, Port, Coastal and Ocean Engineering* vol. 111, no. 2 (1985), pp. 216–234.

[GK96] GOLDMAN, D. and KAPER, T. J. 'Nth-Order Operator Splitting Schemes and Nonreversible Systems'. eng. In: *SIAM journal on numerical analysis* vol. 33, no. 1 (1996), pp. 349–367.

[Hol07] Holthuijsen, L. H. *Waves in oceanic and coastal waters*. eng. Cambridge, 2007.

[Lak+77] Lake, B. M. et al. 'Nonlinear deep-water waves: theory and experiment. Part 2. Evolution of a continuous wave train'. eng. In: *Journal of fluid mechanics* vol. 83, no. 1 (1977), pp. 49–74.

[McL82] McLean, J. W. 'Instabilities of finite-amplitude water waves'. eng. In: *Journal of fluid mechanics* vol. 114, no. 1 (1982), pp. 315–330.

[Mel83] Melville, W. K. 'Wave modulation and breakdown'. eng. In: *Journal of fluid mechanics* vol. 128, no. 1 (1983), pp. 489–506.

[MY80] Martin, D. U. and Yuen, H. C. 'Quasi-recurring energy leakage in the two-space-dimensional nonlinear Schrödinger equation'. In: *The Physics of fluids (1958)* vol. 23, no. 5 (1980), pp. 881–883.

[Sch97] Schwartz, C. 'Nonlinear Operators and their Propagators'. eng. In: (1997).

[TD90] Trulsen, K. and Dysthe, K. B. 'Frequency down-shift through self modulation and breaking.' In: *Water Wave Kinematics*. Ed. by Tørum, A. and Gudmestad, O. T. Kluwer, 1990, pp. 561–572.

[TD97] TRULSEN, K. and DYSTHE, K. B. 'Frequency downshift in three-dimensional wave trains in a deep basin'. eng. In: *Journal of fluid mechanics* vol. 352 (1997), pp. 359–373.

[Tru22] Trulsen, K. 'Stochastic theory'. 2022.

[TSV99] Trulsen, K., Stansberg, C. T. and Velarde, M. G. 'Laboratory evidence of three-dimensional frequency downshift of waves in a long tank'. eng. In: *Physics of fluids (1994)* vol. 11, no. 1 (1999), pp. 235–237.